Energy-Momentum Integrators for Elastic Cosserat Points, Rigid Bodies, and Multibody Systems

Peter Betsch

Abstract The goal of this chapter is to present the development of energy-momentum (EM) schemes in the framework of discrete (or finite-dimensional) mechanical systems. EM integrators belong to the class of structure-preserving numerical methods and have been originally developed in the field of nonlinear solid and structural mechanics. EM schemes and energy dissipating variants thereof typically exhibit improved numerical stability and robustness when compared to standard integrators. Due to their superior numerical properties, EM schemes have soon been extended to more involved applications such as flexible multibody dynamics and coupled thermomechanical problems. In this chapter, we start the development of second-order EM schemes in the context of the Cosserat point (or pseudo-rigid body). The theory of a Cosserat point shares main structural properties with semi-discrete formulations of elastodynamics. Indeed, the Cosserat point can be directly linked to the 4-node tetrahedral finite element. Besides its usefulness in explaining main ingredients of EM schemes such as the algorithmic stress formula, the Cosserat point is ideally suited to perform the transition to rigid body dynamics. In particular, in the present work, the rigid body formulation is obtained by imposing the zero strain condition on the Cosserat point. This way the rigid body is treated as constrained mechanical system. Moreover, we show that the EM discretization of constrained mechanical systems can be derived in a straightforward way from the EM scheme for the Cosserat point. The resulting rigid body formulation is closely connected to natural coordinates. Eventually, we deal with the extension to multibody systems which can be done in a straightforward way due to the presence of holonomic constraints in the present rigid body formulation.

Funding for this work has been provided by the German Science Foundation under Grant BE 2285/10-1.

P. Betsch (✉)
Institute of Mechanics, Karlsruhe Insitute of Technology, Karlsruhe, Germany
e-mail: peter.betsch@kit.edu

P. Betsch (ed.), *Structure-preserving Integrators in Nonlinear Structural Dynamics and Flexible Multibody Dynamics*, CISM International Centre for Mechanical Sciences 565, DOI 10.1007/978-3-319-31879-0_2

1 Introduction

Energy-momentum (EM) integrators have been originally developed in the context of nonlinear structural dynamics. Building upon the previous work by Hughes et al. (1978), Greenspan (1984), Simo and Wong (1991) and Simo et al. (1992b), the first EM scheme for nonlinear elastodynamics has been proposed in the seminal work by Simo and Tarnow (1992). Due to their favorable numerical stability properties (Gonzalez and Simo 1996) EM methods have soon been extended to the realm of nonlinear structural and rigid body dynamics. The description of these systems typically relies on the introduction of rotational coordinates. For example, in rigid body dynamics one may use Euler angles, Euler parameters (or unit quaternions), or Rodrigues parameters for the parametrization of the rotation manifold. It was soon realized that the selection of specific rotational coordinates has a strong impact on the design of structure-preserving integrators (Lewis and Simo 1994). In particular, the use of minimal coordinates (like Euler angles for rigid body dynamics) in general leads to highly nonlinear and elaborate expressions that typically impede the design of time-stepping schemes featuring conservation of angular momentum.

In nonlinear structural dynamics the parametrization of the rotation manifold does affect both the discretization in space and time. It has been shown in Simo et al. (1992a) that the finite element interpolation of rotational variables in general destroys conservation of angular momentum of the semi-discrete system. Strictly speaking the available EM methods for nonlinear beams (Romero and Armero 2002a; Betsch and Steinmann 2003; Leyendecker et al. 2006) and shells (Simo and Tarnow 1994; Brank et al. 1998; Betsch and Sänger 2009a) confine the use of rotational parameters to the nodes of the finite element mesh. Similarly, in these works the discretization in time does not directly rely on the use of rotational parameters.

EM schemes provide a good starting point for the development of energy decaying schemes. Energy decaying variants of EM schemes have been proposed, for example, by Bauchau and Bottasso (1999), Kuhl and Crisfield (1999), Armero and Romero (2001, 2003), Romero and Armero (2002b), Bottasso et al. (2002), Bottasso and Trainelli (2004), Lens and Cardona (2007). More about energy decaying integrators can be found in chapters "High Frequency Dissipative Integration Schemes for Linear and Nonlinear Elastodynamics" and "A Lie Algebra Approach to Lie Group Time Integration of Constrained Systems".

Due to their desirable numerical properties, EM methods have also been extended to more involved problems such as nonlinear visco-elastodynamics (Groß and Betsch 2010), thermo-elastodynamics (Romero 2009; Groß and Betsch 2011; Romero 2010; Hesch and Betsch 2011c; Conde Martín et al. 2016), finite deformation contact problems (Laursen and Chawla 1997; Armero and Petöcz 1998; Hesch and Betsch 2009, 2011b), and flexible multibody dynamics (Bauchau and Bottasso 1999; Ibrahimbegović et al. 2000; Bottasso et al. 2001; Betsch and Steinmann 2002a, c; Lens et al. 2004; Betsch and Sänger 2009b; Leyendecker et al. 2008a). EM schemes have also been incorporated into direct methods for the optimal control of multibody systems (Bottasso and Croce 2004; Betsch et al. 2012; Koch and Leyendecker 2013).

A good account on the development of EM schemes in the context of nonlinear finite element methods can be found in the books by Crisfield (1997), Géradin and Cardona (2001), Laursen (2002), Krenk (2009), Ibrahimbegović (2009), Bauchau (2011).

An alternative route to the design of structure-preserving time-stepping schemes are variational integrators. In the context of multibody dynamics variational integrators have been dealt with, for example, in Leyendecker et al. (2008b), Ober-Blöbaum et al. (2011), Leyendecker et al. (2010), Johnson and Murphey (2009), Betsch et al. (2010). For a tutorial on variational integrators we refer to the chapter "A Brief Introduction to Variational Integrators".

The goal of this chapter is to present the development of EM schemes in the framework of discrete (or finite-dimensional) mechanical systems. To this end, we start in Sect. 2 with the Cosserat point (or pseudo-rigid body). The theory of a Cosserat point shares main structural properties with semi-discrete formulations of elastodynamics. Indeed, the Cosserat point can be directly linked to the 4-node tetrahedral finite element as will be shown in Sect. 2.6. Besides its usefulness in explaining main ingredients of EM schemes such as the algorithmic stress formula, the Cosserat point is ideally suited to perform the transition to rigid body dynamics. In Sect. 3, the rigid body formulation is obtained by imposing the zero strain condition on the Cosserat point. This way the rigid body is treated as constrained mechanical system. Moreover, the EM discretization of constrained mechanical systems can be derived in a straightforward way from the previously developed EM scheme for the Cosserat point. The resulting rigid body formulation is closely connected to natural coordinates as will be shown in Sect. 3.7. Due to the presence of holonomic constraints in the present rigid body formulation, the extension to multibody systems can be done in a straightforward way. This is the subject of Sect. 4. Eventually, in Sect. 5, representative numerical examples are presented.

2 EM Method for Cosserat Points

We start the description of EM schemes in the context of a Cosserat point (Rubin 2000). Similar to the theory of a pseudo-rigid body (Cohen and Muncaster 1988; Nordenholz and O'Reilly 1998) the theory of a Cosserat point represents a finite-dimensional model for a deformable body. This model problem already features key structural properties of more complicated mechanical systems such as nonlinear elastodynamics and structural dynamics. In contrast to the continuum theory the equations governing the motion of a Cosserat point consist of ordinary differential equations (ODEs). Due to its relative simplicity, the theory of a Cosserat point is deemed to be especially well-suited to convey main ideas of the design of EM schemes.

In addition to that, the theory of a Cosserat point paves the way to rigid body dynamics. To this end additional geometric constraints are imposed on the Cosserat point leading to differential-algebraic equations (DAEs) governing the motion of a

rigid body. Consequently, we shall regard the rigid body as a constrained mechanical system. The DAEs not only govern the motion of rigid bodies but also the motion of general flexible multibody systems. It will subsequently become apparent that the development of EM methods for constrained mechanical systems is closely related to the design of EM schemes for elastic bodies.

2.1 Governing Equations

The equations of motion pertaining to the present model problem of a deformable body can be derived from the principle of virtual work for a general deformable continuum. To this end, the assumption of spatially homogeneous deformations is imposed by considering affine deformation maps of the form (Fig. 1)

$$\boldsymbol{x} = \boldsymbol{\Phi}(\boldsymbol{X}, t) = \bar{\boldsymbol{x}}(t) + \boldsymbol{F}(t)(\boldsymbol{X} - \overline{\boldsymbol{X}}) \tag{1}$$

Here, material points in the reference configuration $\mathcal{B} \subset \mathbb{R}^3$ are denoted by $\boldsymbol{X} \in \mathcal{B}$, $\overline{\boldsymbol{X}} \in \mathcal{B}$ is the center of mass, and $\bar{\boldsymbol{x}}(t) \in \mathcal{B}_t$ denotes the corresponding placement in the configuration $\mathcal{B}_t \subset \mathbb{R}^3$ at time $t \in [0, T]$, the time interval of interest. Moreover, $\boldsymbol{F}(t) = D\boldsymbol{\Phi}_t(\boldsymbol{X})$ is the deformation gradient, where $\boldsymbol{\Phi}_t(\boldsymbol{X}) = \boldsymbol{\Phi}(\boldsymbol{X}, t)$.

Due to the kinematic assumption (1) the deformation gradient $\boldsymbol{F}$ does not depend on $\boldsymbol{X}$. This property gives rise to the present model problem of a Cosserat point. Alternatively, the model problem could be termed *homogeneous elasticity* (see, for example, Simo et al. 1991). Another perspective is to view the present model problem as an extension of the classical model of a rigid body. This viewpoint leads to the notion of a pseudo-rigid body. The configuration space of the free Cosserat point is given by

$$\mathsf{Q} = \left\{(\bar{\boldsymbol{x}}, \boldsymbol{F}) \in \mathbb{R}^3 \times \mathbb{R}^{3\times 3} \mid \det(\boldsymbol{F}) > 0\right\} \tag{2}$$

Note that $\boldsymbol{F} \in GL^+(3)$, where $GL^+(3)$ is the subgroup of the general linear group, $GL(3)$, consisting of 3×3 matrices with positive determinant. Obviously, $\dim(\mathsf{Q}) = 12$, so that the free Cosserat point has $n = 12$ degrees of freedom (DOFs). We further remark that consistent with the definition of the center of mass in the reference configuration we have the relationships

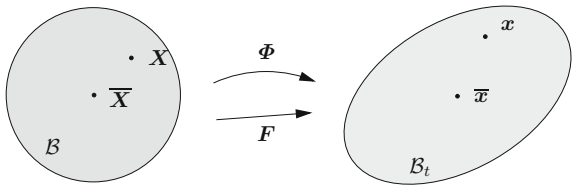

Fig. 1 Planar illustration of the Cosserat point: Reference configuration $\mathcal{B}$ (*left*), and current configuration $\mathcal{B}_t$ (*right*)

$$\overline{\boldsymbol{X}} = \frac{1}{M}\int_{\mathcal{B}_0} \rho_0 \boldsymbol{X}\, dV \qquad \text{or} \qquad \int_{\mathcal{B}_0} \rho_0 (\boldsymbol{X} - \overline{\boldsymbol{X}})\, dV = \boldsymbol{0}$$

where $M = \int_{\mathcal{B}_0} \rho_0\, dV$ is the total mass and $\rho_0 : \mathcal{B}_0 \to \mathbb{R}$ is the reference density. The principle of virtual work for a general continuum body can be written as

$$G(\boldsymbol{\Phi}; \delta\boldsymbol{\Phi}) = G_{\text{dyn}}(\boldsymbol{\Phi}; \delta\boldsymbol{\Phi}) + G_{\text{int}}(\boldsymbol{\Phi}; \delta\boldsymbol{\Phi}) - G_{\text{ext}}(\boldsymbol{\Phi}; \delta\boldsymbol{\Phi}) = 0 \tag{3}$$

where $\delta\boldsymbol{\Phi} : \mathcal{B}_0 \to \mathbb{R}^3$ can be interpreted as virtual displacement of the material point $\boldsymbol{X}$, G_{ext} is the virtual work of the external loading, G_{int} is the internal virtual work due to deformation, and G_{dyn} is the contribution of the inertia terms. In particular

$$G_{\text{dyn}}(\boldsymbol{\Phi}; \delta\boldsymbol{\Phi}) = \int_{\mathcal{B}_0} \rho_0 \delta\boldsymbol{\Phi} \cdot \ddot{\boldsymbol{\Phi}}\, dV \tag{4}$$

where $\ddot{\boldsymbol{\Phi}} = \frac{\partial^2}{\partial t^2}\boldsymbol{\Phi}(\boldsymbol{X}, t)$ is the acceleration of the material point $\boldsymbol{X}$ at time t. The virtual work of the internal forces is given by

$$G_{\text{int}}(\boldsymbol{\Phi}; \delta\boldsymbol{\Phi}) = \int_{\mathcal{B}_0} \delta\boldsymbol{F} : \boldsymbol{P}\, dV \tag{5}$$

where $\delta\boldsymbol{F} = D\delta\boldsymbol{\Phi}(\boldsymbol{X})$, and $\boldsymbol{P}$ is the first Piola–Kirchhoff stress tensor. Note that $\boldsymbol{P} = \boldsymbol{F}\boldsymbol{S}$, where $\boldsymbol{S}$ is the second Piola–Kirchhoff stress tensor. We further remark that the scalar product of the two second-order tensors $\delta\boldsymbol{F}$ and $\boldsymbol{P}$ is given by

$$\delta\boldsymbol{F} : \boldsymbol{P} = \text{tr}(\delta\boldsymbol{F}^T\boldsymbol{P})$$

where $\text{tr}(\bullet)$ is the trace operator and $\delta\boldsymbol{F}^T$ denotes the transpose of $\delta\boldsymbol{F}$. The virtual work of the external loading can be written as

$$G_{\text{ext}}(\boldsymbol{\Phi}; \delta\boldsymbol{\Phi}) = \int_{\mathcal{B}_0} \rho_0 \delta\boldsymbol{\Phi} \cdot \boldsymbol{b}\, dV + \int_{\partial\mathcal{B}_0} \delta\boldsymbol{\Phi} \cdot \boldsymbol{p}\, dA \tag{6}$$

where $\boldsymbol{b} : \mathcal{B}_0 \times [0, T] \to \mathbb{R}^3$ is the body force per unit mass and $\boldsymbol{p} : \partial\mathcal{B}_0 \times [0, T] \to \mathbb{R}^3$ is the nominal traction vector on the boundary. For simplicity of exposition we confine our attention to the pure Neumann problem (i.e., no Dirichlet boundary conditions).

To derive the variational formulation of the present model problem we insert (1) along with

$$\delta\boldsymbol{\Phi}(\boldsymbol{X}) = \delta\overline{\boldsymbol{x}} + \delta\boldsymbol{F}(\boldsymbol{X} - \overline{\boldsymbol{X}}) \tag{7}$$

into the principle of virtual work (3). Accordingly, the virtual work of the inertia terms (4) yields

$$\hat{G}_{\text{dyn}}\big((\overline{\boldsymbol{x}}, \boldsymbol{F}); (\delta\overline{\boldsymbol{x}}, \delta\boldsymbol{F})\big) = \delta\overline{\boldsymbol{x}} \cdot M\ddot{\overline{\boldsymbol{x}}} + \delta\boldsymbol{F} : (\ddot{\boldsymbol{F}}\boldsymbol{E}_0) \tag{8}$$

where $\boldsymbol{E}_0$ is the constant and positive-definite tensor given by

$$\boldsymbol{E}_0 = \int_{\mathcal{B}_0} \rho_0 (\boldsymbol{X} - \overline{\boldsymbol{X}}) \otimes (\boldsymbol{X} - \overline{\boldsymbol{X}})\, dV \tag{9}$$

Note that $\otimes$ is the standard tensor product of two vectors. Tensor (9) is often called the (referential) *Euler tensor* (Gurtin 1981), and is closely related to the classical inertia tensor of rigid body dynamics, see Sect. 3.4 for further details.

Concerning the internal virtual work (5) the assumption of an homogeneous deformation leads to the expression

$$\hat{G}_{\text{int}}(\boldsymbol{F}; \delta\boldsymbol{F}) = \delta\boldsymbol{F} : \left(\boldsymbol{F} \int_{\mathcal{B}_0} \boldsymbol{S}(\boldsymbol{F})\, dV \right) \tag{10}$$

where an elastic solid with stress response function $\boldsymbol{S}(\boldsymbol{F})$ has been assumed. In the following we focus on constitutive models for hyperelastic solids. In particular, a frame-indifferent hyperelastic stress response is given by

$$\boldsymbol{S}(\boldsymbol{F}) = 2DW(\boldsymbol{C}) \tag{11}$$

where W denotes the strain energy density and $\boldsymbol{C} = \boldsymbol{F}^T\boldsymbol{F}$ is the right Cauchy–Green deformation tensor. Expression (10) shows that only the stress resultants

$$\overline{\boldsymbol{S}} = \int_{\mathcal{B}_0} \boldsymbol{S}\, dV = 2V_0 DW(\boldsymbol{C}) \tag{12}$$

enter the internal virtual work. Here $V_0 = \int_{\mathcal{B}_0} dV$ is the total volume of the body in the reference configuration. We further introduce the total strain energy given by

$$U = \int_{\mathcal{B}_0} W(\boldsymbol{C})\, dV = V_0 W(\boldsymbol{C}) \tag{13}$$

so that the second Piola–Kirchhoff stress resultants (12) can be written as

$$\overline{\boldsymbol{S}} = 2DU(\boldsymbol{C}) \tag{14}$$

Now the internal virtual work pertaining to the hyperelastic Cosserat point can be written as

$$\hat{G}_{\text{int}}(\boldsymbol{F}; \delta\boldsymbol{F}) = \delta\boldsymbol{F} : \big(2\boldsymbol{F}DU(\boldsymbol{C})\big) \tag{15}$$

The virtual work of the external loading (6) together with (7) yields

$$\hat{G}_{\text{ext}}\big((\overline{\boldsymbol{x}}, \boldsymbol{F}); (\delta\overline{\boldsymbol{x}}, \delta\boldsymbol{F})\big) = \delta\overline{\boldsymbol{x}} \cdot \boldsymbol{f}_{\text{ext}} + \delta\boldsymbol{F} : \boldsymbol{M}_{\text{ext}} \tag{16}$$

where

$$\boldsymbol{f}_{\text{ext}} = \int_{\mathcal{B}_0} \rho_0 \boldsymbol{b}\, dV + \int_{\partial\mathcal{B}_0} \boldsymbol{p}\, dA \tag{17}$$

$$\boldsymbol{M}_{\text{ext}} = \int_{\mathcal{B}_0} \rho_0 \boldsymbol{b} \otimes (\boldsymbol{X} - \overline{\boldsymbol{X}})\, dV + \int_{\partial\mathcal{B}_0} \boldsymbol{p} \otimes (\boldsymbol{X} - \overline{\boldsymbol{X}})\, dA \tag{18}$$

Note that $\boldsymbol{f}_{\text{ext}}$ is the resultant external force acting on the body. Moreover, $\boldsymbol{M}_{\text{ext}}$ may be called *referential external force-moment* (Cohen and Muncaster 1988) relative to the center of mass. Altogether the variational formulation emanating from the principle of virtual work (3) can be written as

$$\delta\overline{\boldsymbol{x}} \cdot \left(M\ddot{\overline{\boldsymbol{x}}} - \boldsymbol{f}_{\text{ext}}\right) + \delta\boldsymbol{F} : \left(\ddot{\boldsymbol{F}}\boldsymbol{E}_0 + 2\boldsymbol{F}DU(\boldsymbol{C}) - \boldsymbol{M}_{\text{ext}}\right) = 0 \tag{19}$$

The last equation has to hold for arbitrary $\delta\overline{\boldsymbol{x}} \in \mathbb{R}^3$ and $\delta\boldsymbol{F} \in \mathbb{R}^{3\times3}$. These equations give rise to the following initial value problem: Find $\overline{\boldsymbol{x}} : [0, T] \to \mathbb{R}^3$ and $\boldsymbol{F} : [0, T] \to \mathbb{R}^{3\times3}$ such that

$$\begin{aligned} M\ddot{\overline{\boldsymbol{x}}} &= \boldsymbol{f}_{\text{ext}} \\ \ddot{\boldsymbol{F}}\boldsymbol{E}_0 + 2\boldsymbol{F}DU(\boldsymbol{C}) &= \boldsymbol{M}_{\text{ext}} \end{aligned} \tag{20}$$

subject to the initial conditions $\overline{\boldsymbol{x}}(0) = \overline{\boldsymbol{x}}_0$, $\dot{\overline{\boldsymbol{x}}}(0) = \overline{\boldsymbol{v}}_0$, $\boldsymbol{F}(0) = \boldsymbol{F}_0$, and $\dot{\boldsymbol{F}}(0) = \boldsymbol{V}_0$, where $\overline{\boldsymbol{x}}_0, \overline{\boldsymbol{v}}_0 \in \mathbb{R}^3$ and $\boldsymbol{F}_0, \boldsymbol{V}_0 \in \mathbb{R}^{3\times3}$ are given quantities. The above ODEs coincide with the *equations of motion in referential form* in Cohen and Muncaster (1988).

2.1.1 Balance Laws

Before dealing with the balance laws we recast (19) in an alternative form. Note, however, that the balance laws for linear momentum, angular momentum, and energy can be directly deduced from the principle of virtual work in the form (19) as well. For completeness, this procedure is outlined in Appendix A.1.

2.2 Formulation in Terms of Directors

For our purposes it is convenient to recast the previously derived equations of motion in a form that is typically used in the theory of a Cosserat point (Rubin 2000). To this end we write the homogeneous deformation gradient as

$$\boldsymbol{F}(t) = \boldsymbol{d}_i(t) \otimes \boldsymbol{D}^i \tag{21}$$

where $\boldsymbol{d}_i(t) \in \mathbb{R}^3$ are three director vectors that in general rotate, stretch and shear with the body in its motion (Fig. 2). Note that in the last equation and in what follows, the summation convention applies to indices appearing twice in a formula. The directors are subject to the requirement that $(\boldsymbol{d}_1 \times \boldsymbol{d}_2) \cdot \boldsymbol{d}_3 > 0$, which is consistent with the condition $\det(\boldsymbol{F}) > 0$.

Corresponding to the directors $\boldsymbol{d}_i(t) \in \mathbb{R}^3$, we introduce the vectors $\boldsymbol{D}_i \in \mathbb{R}^3$ constituting the director triad in the reference configuration. In particular, $\boldsymbol{D}_i$ represent a basis fixed in space whose origin coincides with the center of mass. The corresponding coordinates will be denoted by

$$X^i = \boldsymbol{D}^i \cdot (\boldsymbol{X} - \overline{\boldsymbol{X}}) \tag{22}$$

Without loss of generality, we assume that the directors in the reference configuration are mutually orthonormal, that is, $\boldsymbol{D}^i \cdot \boldsymbol{D}^j = \delta^{ij}$, where δ^{ij} is the Kronecker delta. Note that the last assumption implies $\boldsymbol{D}_i = \boldsymbol{D}^i$. We further assume that the reference configuration of the Cosserat point is a natural (i.e., stress-free) configuration. Inserting (21) into (1) and taking into account (22) yields

$$\boldsymbol{x} = \overline{\boldsymbol{x}}(t) + X^i \boldsymbol{d}_i(t) \tag{23}$$

The last equation indicates that the kinematics of the Cosserat point confines the (convected) coordinates X^i to remain straight. Differentiating (21) with respect to time gives

$$\begin{aligned} \dot{\boldsymbol{F}}(t) &= \dot{\boldsymbol{d}}_i(t) \otimes \boldsymbol{D}^i \\ \ddot{\boldsymbol{F}}(t) &= \ddot{\boldsymbol{d}}_i(t) \otimes \boldsymbol{D}^i \end{aligned} \tag{24}$$

In line with (7) we further have

$$\delta \boldsymbol{F} = \delta \boldsymbol{d}_i \otimes \boldsymbol{D}^i \tag{25}$$

Now we are in a position to recast the ODEs (20) governing the motion of the Cosserat point in an alternative form. Substituting (25) along with $(24)_2$ into the virtual work (8) of the inertia terms we obtain

$$\tilde{G}_{\text{dyn}}\big((\overline{\boldsymbol{x}}, \boldsymbol{d}_i); (\delta\overline{\boldsymbol{x}}, \delta\boldsymbol{d}_i)\big) = \delta\overline{\boldsymbol{x}} \cdot M\ddot{\overline{\boldsymbol{x}}} + \delta\boldsymbol{d}_i \cdot E_0^{ij}\ddot{\boldsymbol{d}}_j \tag{26}$$

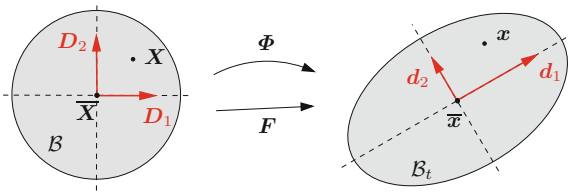

Fig. 2 Planar illustration of the Cosserat point: Reference configuration $\mathcal{B}$ (*left*), and current configuration $\mathcal{B}_t$ (*right*)

where the components E_0^{ij} of the referential Euler tensor (9) are given by

$$E_0^{ij} = \boldsymbol{D}^i \cdot \boldsymbol{E}_0 \boldsymbol{D}^j = \int_{\mathcal{B}_0} \rho_0 X^i X^j \, dV \tag{27}$$

In the last equation use has been made of (9) and (22). Similarly, expression (15) for the internal virtual work can be recast in the form

$$\tilde{G}_{\text{int}}(\boldsymbol{d}; \delta \boldsymbol{d}_i) = \delta \boldsymbol{d}_i \cdot \boldsymbol{d}_j \, (\boldsymbol{D}^i \cdot 2DU(\boldsymbol{C})\boldsymbol{D}^j) \tag{28}$$

where use has been made of (13). Note that the strain energy $U(\boldsymbol{C})$ depends on the right Cauchy–Green deformation tensor $\boldsymbol{C} = \boldsymbol{F}^T \boldsymbol{F}$ which, in view of (21), can also be written as

$$\boldsymbol{C} = d_{ij} \boldsymbol{D}^i \otimes \boldsymbol{D}^j$$

where

$$d_{ij} = \boldsymbol{d}_i \cdot \boldsymbol{d}_j \tag{29}$$

play the role of metric coefficients. Accordingly, we have six independent metric coefficients measuring homogeneous deformations of the Cosserat point. Specifically, if the magnitude of $\boldsymbol{d}_i$ changes, the Cosserat point experiences extension, whereas shear deformation happens if the angle between any two directors changes. Next consider

$$\tfrac{d}{dt} U(\boldsymbol{C}) = DU(\boldsymbol{C}) : \dot{\boldsymbol{C}} = DU(\boldsymbol{C}) : (\dot{d}_{ij} \boldsymbol{D}^i \otimes \boldsymbol{D}^j) = \tfrac{1}{2} \overline{S}^{ij} \dot{d}_{ij} \tag{30}$$

where the components

$$\overline{S}^{ij} = \boldsymbol{D}^i \cdot 2DU(\boldsymbol{C})\boldsymbol{D}^i = 2 \frac{\partial U}{\partial d_{ij}} \tag{31}$$

have been introduced. Moreover, employing (29) in (30) yields the relationship

$$\tfrac{d}{dt} U(\boldsymbol{C}) = \tfrac{1}{2} \overline{S}^{ij} (\dot{\boldsymbol{d}}_i \cdot \boldsymbol{d}_j + \boldsymbol{d}_i \cdot \dot{\boldsymbol{d}}_j) = \overline{S}^{ij} \boldsymbol{d}_j \cdot \dot{\boldsymbol{d}}_i \tag{32}$$

where the symmetry of $\overline{S}^{ij}$ (i.e., $\overline{S}^{ij} = \overline{S}^{ji}$) has been taken into account. Next we introduce the internal director forces

$$\boldsymbol{f}^i_{\text{int}} = \overline{S}^{ij} \boldsymbol{d}_j = \frac{\partial U}{\partial \boldsymbol{d}_i} \tag{33}$$

such that the internal virtual work (28) can be written as

$$\tilde{G}_{\text{int}}(\boldsymbol{d}; \delta \boldsymbol{d}_i) = \delta \boldsymbol{d}_i \cdot \boldsymbol{f}^i_{\text{int}} \tag{34}$$

Remark 2.1 For later use we note that applying the chain rule and taking into account the symmetry of the metric coefficients d_{jk} one gets

$$\begin{aligned}\frac{\partial U}{\partial \boldsymbol{d}_i} &= \frac{\partial U}{\partial d_{jk}}\frac{\partial d_{jk}}{\partial \boldsymbol{d}_i} \\ &= \frac{\partial U}{\partial d_{jk}}\left(\delta^i_j \boldsymbol{d}_k + \delta^i_k \boldsymbol{d}_j\right) \\ &= 2\frac{\partial U}{\partial d_{ik}}\boldsymbol{d}_k\end{aligned} \tag{35}$$

This result is consistent with (31) and (33).

The virtual work of the external loading (16) can be written as

$$\tilde{G}_{\text{ext}}\big((\overline{\boldsymbol{x}}, \boldsymbol{d}_i); (\delta\overline{\boldsymbol{x}}, \delta\boldsymbol{d}_i)\big) = \delta\overline{\boldsymbol{x}} \cdot \boldsymbol{f}_{\text{ext}} + \delta\boldsymbol{d}_i \cdot \boldsymbol{f}^i_{\text{ext}} \tag{36}$$

where the external director forces $\boldsymbol{f}^i_{\text{ext}} \in \mathbb{R}^3$ are given by

$$\boldsymbol{f}^i_{\text{ext}} = \boldsymbol{M}_{\text{ext}}\boldsymbol{D}^i = \int_{\mathcal{B}_0} \rho_0 X^i \boldsymbol{b}\, dV + \int_{\partial\mathcal{B}_0} X^i \boldsymbol{p}\, dA \tag{37}$$

To get the last equation use has been made of (18) along with (22). Note that with regard to the last equation the referential external force-moment $\boldsymbol{M}_{\text{ext}}$ defined in (18) can also be written as

$$\boldsymbol{M}_{\text{ext}} = \boldsymbol{f}^i_{\text{ext}} \otimes \boldsymbol{D}_i \tag{38}$$

Now, using (26), (34), and (36), a variational formulation of the Cosserat point equivalent to (19) can be obtained:

$$\delta\overline{\boldsymbol{x}} \cdot \left(M\ddot{\overline{\boldsymbol{x}}} - \boldsymbol{f}_{\text{ext}}\right) + \delta\boldsymbol{d}_i \cdot \left(E^{ij}_0 \ddot{\boldsymbol{d}}_j + \boldsymbol{f}^i_{\text{int}} - \boldsymbol{f}^i_{\text{ext}}\right) = 0 \tag{39}$$

Due to the arbitrariness of $\delta\overline{\boldsymbol{x}} \in \mathbb{R}^3$ and $\delta\boldsymbol{d}_i \in \mathbb{R}^3$, $i = 1, 2, 3$, we obtain 12 independent ODEs giving rise to the following initial value problem for the hyperelastic Cosserat point: Find $\overline{\boldsymbol{x}} : [0, T] \to \mathbb{R}^3$ and $\boldsymbol{d}_i : [0, T] \to \mathbb{R}^3$ $(i = 1, 2, 3)$ such that

$$\begin{aligned} M\ddot{\overline{\boldsymbol{x}}} &= \boldsymbol{f}_{\text{ext}} \\ E^{ij}_0 \ddot{\boldsymbol{d}}_j + \boldsymbol{f}^i_{\text{int}} &= \boldsymbol{f}^i_{\text{ext}} \end{aligned} \tag{40}$$

subject to the initial conditions $\overline{\boldsymbol{x}}(0) = \overline{\boldsymbol{x}}_0$, $\dot{\overline{\boldsymbol{x}}}(0) = \overline{\boldsymbol{v}}_0$, $\boldsymbol{d}_i(0) = (\boldsymbol{d}_i)_0$, and $\dot{\boldsymbol{d}}_i(0) = (\boldsymbol{v}_i)_0$, where $\overline{\boldsymbol{x}}_0, \overline{\boldsymbol{v}}_0, (\boldsymbol{d}_i)_0, (\boldsymbol{v}_i)_0 \in \mathbb{R}^3$ are given quantities. It is worth noting that the ODEs $(40)_2$ coincide with the *balances of director momentum* in Rubin (2000). Moreover, in Rubin (2000), $\boldsymbol{f}^i_{\text{ext}} \in \mathbb{R}^3$ and $\boldsymbol{f}^i_{\text{int}} \in \mathbb{R}^3$ are called *external director couples* and *intrinsic director couples*, respectively.

2.3 Balance of Linear Momentum

The balance law for linear momentum can be directly obtained from the principle of virtual work (39) by setting $\delta\bar{\boldsymbol{x}} = \boldsymbol{\xi}$, where $\boldsymbol{\xi} \in \mathbb{R}^3$ is a constant vector, together with $\delta \boldsymbol{d}_i = \boldsymbol{0}$. Accordingly, we get

$$\frac{d}{dt}\boldsymbol{l} = \boldsymbol{f}_{\text{ext}} \tag{41}$$

where the total linear momentum of the Cosserat point is given by

$$\boldsymbol{l} = M\dot{\bar{\boldsymbol{x}}} \tag{42}$$

As before, the right-hand side of (41) characterizes the resultant external force applied to the Cosserat point.

2.4 Balance of Angular Momentum

In preparation for the design of EM integrators, we next consider the fundamental balance law for angular momentum. Substituting $\delta\bar{\boldsymbol{x}} = \boldsymbol{\xi} \times \bar{\boldsymbol{x}}$ along with $\delta \boldsymbol{d}_i = \boldsymbol{\xi} \times \boldsymbol{d}_i$ into (39) yields

$$(\boldsymbol{\xi} \times \bar{\boldsymbol{x}}) \cdot \left(M\ddot{\bar{\boldsymbol{x}}} - \boldsymbol{f}_{\text{ext}}\right) + (\boldsymbol{\xi} \times \boldsymbol{d}_i) \cdot \left(E_0^{ij}\ddot{\boldsymbol{d}}_j + \boldsymbol{f}_{\text{int}}^i - \boldsymbol{f}_{\text{ext}}^i\right) = 0 \tag{43}$$

or

$$\boldsymbol{\xi} \cdot \left(M\bar{\boldsymbol{x}} \times \ddot{\bar{\boldsymbol{x}}} - \bar{\boldsymbol{x}} \times \boldsymbol{f}_{\text{ext}} + E_0^{ij}\boldsymbol{d}_i \times \ddot{\boldsymbol{d}}_j + \bar{S}^{ij}\boldsymbol{d}_i \times \boldsymbol{d}_j - \boldsymbol{d}_i \times \boldsymbol{f}_{\text{ext}}^i\right) = 0 \tag{44}$$

In the last equation use has been made of (33). Due to the symmetry of $\bar{S}^{ij}$ and the skew-symmetry of the vector cross product we have $\bar{S}^{ij}\boldsymbol{d}_i \times \boldsymbol{d}_j = \boldsymbol{0}$. Now equation (44) can be recast in the form

$$\frac{d}{dt}\boldsymbol{j} = \boldsymbol{m}_{\text{ext}} \tag{45}$$

where $\boldsymbol{j} \in \mathbb{R}^3$ is the total angular momentum of the Cosserat point and $\boldsymbol{m}_{\text{ext}} \in \mathbb{R}^3$ is the resultant external torque acting on the Cosserat point:

$$\begin{aligned} \boldsymbol{j} &= M\bar{\boldsymbol{x}} \times \dot{\bar{\boldsymbol{x}}} + E_0^{ij}\boldsymbol{d}_i \times \dot{\boldsymbol{d}}_j \\ \boldsymbol{m}_{\text{ext}} &= \bar{\boldsymbol{x}} \times \boldsymbol{f}_{\text{ext}} + \boldsymbol{d}_i \times \boldsymbol{f}_{\text{ext}}^i \end{aligned} \tag{46}$$

Note that both quantities are referred to the origin of the inertial frame of reference.

2.5 Balance of Energy

The balance law for energy can be obtained from the variational formulation (39) by substituting $\dot{\bar{\boldsymbol{x}}}$ for $\delta\bar{\boldsymbol{x}}$ and $\dot{\boldsymbol{d}}_i$ for $\delta\boldsymbol{d}_i$. Accordingly, we get

$$\dot{\bar{\boldsymbol{x}}} \cdot \left(M\ddot{\bar{\boldsymbol{x}}} - \boldsymbol{f}_{\text{ext}}\right) + \dot{\boldsymbol{d}}_i \cdot \left(E_0^{ij}\ddot{\boldsymbol{d}}_j + \frac{\partial U}{\partial \boldsymbol{d}_i} - \boldsymbol{f}^i_{\text{ext}}\right) = 0$$

where (33) has been employed. The last equation can be recast in the form

$$\frac{d}{dt}E = P_{\text{ext}} \tag{47}$$

where

$$P_{\text{ext}} = \boldsymbol{f}_{\text{ext}} \cdot \dot{\bar{\boldsymbol{x}}} + \boldsymbol{f}^i_{\text{ext}} \cdot \dot{\boldsymbol{d}}_i \tag{48}$$

denotes the power of the external forces acting on the body. Moreover, E is the total mechanical energy[1] given by

$$E = T + U \tag{49}$$

where U denotes the total strain energy defined in (13) and

$$T = \frac{1}{2}M\dot{\bar{\boldsymbol{x}}} \cdot \dot{\bar{\boldsymbol{x}}} + \frac{1}{2}E_0^{ij}\dot{\boldsymbol{d}}_i \cdot \dot{\boldsymbol{d}}_j \tag{50}$$

is the kinetic energy of the Cosserat point.

Remark 2.2 It is obvious from the balance law (45) that the total angular momentum is conserved (or a first integral of the motion) if the resultant external torque vanishes, that is, if $\boldsymbol{m}_{\text{ext}} = \boldsymbol{0}$. Then (43) yields

$$\begin{aligned} \boldsymbol{\xi} \cdot \left(M\bar{\boldsymbol{x}} \times \dddot{\bar{\boldsymbol{x}}} + E_0^{ij}\boldsymbol{d}_i \times \ddot{\boldsymbol{d}}_j\right) &= \boldsymbol{\xi} \cdot \left(\boldsymbol{d}_i \times \tfrac{\partial U}{\partial \boldsymbol{d}_i}\right) \\ \boldsymbol{\xi} \cdot \tfrac{d}{dt}\boldsymbol{j} &= \boldsymbol{\xi} \cdot \left(\bar{S}^{ij}\boldsymbol{d}_i \times \boldsymbol{d}_j\right) \\ &= 0 \end{aligned} \tag{51}$$

where use has been made of (33). Due to the arbitrariness of $\boldsymbol{\xi} \in \mathbb{R}^3$ the last equality implies that $\boldsymbol{j}$ is constant.

Remark 2.3 According to Noether's theorem conservation laws are intimately connected with invariance (or symmetry) properties of the system. In the present case conservation of angular momentum can be linked to the invariance of the potential energy under rotations.

[1] If the external loads or part of them can be derived from an associated potential energy function V_{ext} their contribution to the balance of energy can be shifted to the left-hand side of (47) by replacing U in (49) with $U + V_{\text{ext}}$.

In essence, the principle of material frame-indifference requires the stress response to be invariant under rigid motions. This requirement is satisfied by the fact that the total strain energy (13) is a function of the metric coefficients (29). That is,

$$U = \hat{U}(\boldsymbol{d}_i) = \tilde{U}(d_{ij}) \tag{52}$$

This implies invariance under rotations. To see this, let $\boldsymbol{d}_i^\sharp(t)$ define a motion that differs from $\boldsymbol{d}_i(t)$ by a rotation. Then, there is a rotation tensor $\boldsymbol{Q}(t) \in \mathrm{SO}(3)$ that belongs to the Special Orthogonal group in 3-space such that

$$\boldsymbol{d}_i^\sharp = \boldsymbol{Q}\boldsymbol{d}_i$$

It can be easily seen that the metric coefficients d_{ij} are invariant under rotations:

$$\begin{aligned} d_{ij}^\sharp &= \boldsymbol{d}_i^\sharp \cdot \boldsymbol{d}_j^\sharp \\ &= (\boldsymbol{Q}\boldsymbol{d}_i) \cdot \boldsymbol{Q}\boldsymbol{d}_j \\ &= \boldsymbol{d}_i \cdot \boldsymbol{Q}^T\boldsymbol{Q}\boldsymbol{d}_j \\ &= \boldsymbol{d}_i \cdot \boldsymbol{d}_j \\ &= d_{ij} \end{aligned} \tag{53}$$

With regard to (52) this implies rotational invariance of the total strain energy:

$$\hat{U}(\boldsymbol{Q}\boldsymbol{d}_i) = \hat{U}(\boldsymbol{d}_i) \tag{54}$$

Let $\boldsymbol{Q}_\varepsilon = \exp_{\mathrm{SO}(3)}(\varepsilon\widehat{\boldsymbol{\xi}}) \in \mathrm{SO}(3)$ for any $\varepsilon \in \mathbb{R}$ and skew-symmetric tensor $\widehat{\boldsymbol{\xi}} \in \mathrm{so}(3)$. In this connection, $\exp_{\mathrm{SO}(3)} : \mathrm{so}(3) \mapsto \mathrm{SO}(3)$ is the exponential map on the rotation group SO(3), given by the Rodrigues formula (see, for example, Marsden and Ratiu 1999)

$$\exp_{\mathrm{SO}(3)}(\varepsilon\widehat{\boldsymbol{\xi}}) = \boldsymbol{I} + \frac{\sin(\varepsilon\|\boldsymbol{\xi}\|)}{\|\boldsymbol{\xi}\|}\widehat{\boldsymbol{\xi}} + \frac{1}{2}\left[\frac{\sin(\varepsilon\|\boldsymbol{\xi}\|/2)}{\|\boldsymbol{\xi}/2\|}\right]^2\widehat{\boldsymbol{\xi}}^2 \tag{55}$$

Here, $\widehat{\boldsymbol{\xi}} \in \mathrm{so}(3)$ is a skew-symmetric tensor with associated axial vector $\boldsymbol{\xi} \in \mathbb{R}^3$. That is, $\widehat{\boldsymbol{\xi}}\boldsymbol{a} = \boldsymbol{\xi} \times \boldsymbol{a}$ for any $\boldsymbol{a} \in \mathbb{R}^3$. It can be easily verified that $\boldsymbol{Q}_\varepsilon = \exp_{\mathrm{SO}(3)}(\varepsilon\widehat{\boldsymbol{\xi}})$ satisfies

$$\boldsymbol{Q}_{\varepsilon=0} = \boldsymbol{I} \qquad \text{and} \qquad \left.\frac{d}{d\varepsilon}\right|_{\varepsilon=0} \boldsymbol{Q}_\varepsilon = \widehat{\boldsymbol{\xi}}$$

Rotational invariance of the strain energy function (54) yields

$$\begin{aligned} 0 &= \left.\tfrac{d}{d\varepsilon}\right|_{\varepsilon=0} \hat{U}\left(\boldsymbol{Q}_\varepsilon\boldsymbol{d}_i\right) \\ &= \tfrac{\partial\hat{U}}{\partial\boldsymbol{d}_i} \cdot \widehat{\boldsymbol{\xi}}\boldsymbol{d}_i \\ &= -\boldsymbol{\xi} \cdot \left(\tfrac{\partial\hat{U}}{\partial\boldsymbol{d}_i} \times \boldsymbol{d}_i\right) \end{aligned} \tag{56}$$

for any $\boldsymbol{\xi} \in \mathbb{R}^3$. Comparison of the last equation with $(51)_1$ shows that rotational invariance of the strain energy indeed yields the conservation law for angular momentum.

Remark 2.4 The rotational invariance of the total strain energy (52) is in agreement with Cauchy's representation theorem (see Truesdell and Noll 2004, Sect. 11, or Antman 2005, Chapter 8). Accordingly, if a scalar-valued function $\hat{f}(\boldsymbol{d}_i)$ is invariant under the proper orthogonal group then it depends only on the set of invariants $\mathbb{S}(\eta) \cup \mathbb{T}(\eta)$, where η denotes the ordered set of directors $\eta = \{\boldsymbol{d}_1, \boldsymbol{d}_2, \boldsymbol{d}_3\}$ and

$$\begin{aligned} \mathbb{S}(\eta) &= \{\boldsymbol{d}_i \cdot \boldsymbol{d}_j, 1 \leq i \leq j \leq 3\} \\ \mathbb{T}(\eta) &= \{(\boldsymbol{d}_1 \times \boldsymbol{d}_2) \cdot \boldsymbol{d}_3\} \end{aligned}$$

The fact that the metric coefficients $d_{ij} \in \mathbb{S}(\eta)$ corroborates that the total strain energy $\hat{U}(\boldsymbol{d}_i) = \tilde{U}(d_{ij})$ is invariant under rotations.

2.6 The Link to Finite Elements

The initial value problem (40) fits into the standard framework for semi-discrete mechanical systems resulting from a space discretization of nonlinear elastodynamics. The finite element method is commonly used to perform the discretization in space of continuum bodies. This results in the semi-discrete equations of motion which assume the standard form

$$\boldsymbol{M}\ddot{\boldsymbol{q}} + \boldsymbol{F}_{\text{int}}(\boldsymbol{q}) = \boldsymbol{F}_{\text{ext}}(\boldsymbol{q}) \tag{57}$$

The system of nonlinear second-order ODEs (57) is subject to the initial conditions $\boldsymbol{q}(0) = \boldsymbol{q}_0$ and $\dot{\boldsymbol{q}}(0) = \boldsymbol{v}_0$, where $\boldsymbol{q}_0, \boldsymbol{v}_0 \in \mathbb{R}^n$ are given. For the free hyperelastic Cosserat point we have $n = 12$ DOFs. In particular, the configuration vector $\boldsymbol{q} : [0, T] \to \mathbb{R}^n$ of the Cosserat point is given by

$$\boldsymbol{q} = \begin{bmatrix} \boldsymbol{q}_1 \\ \vdots \\ \boldsymbol{q}_N \end{bmatrix} = \begin{bmatrix} \bar{\boldsymbol{x}} \\ \boldsymbol{d}_1 \\ \boldsymbol{d}_2 \\ \boldsymbol{d}_3 \end{bmatrix} \tag{58}$$

where N denotes the number of 'nodal' configuration vectors $\boldsymbol{q}_A \in \mathbb{R}^3$ needed to describe the finite-dimensional mechanical system at hand. Obviously, for the Cosserat point we have $N = 4$. Taking into account the above partition of the configuration vector $\boldsymbol{q} \in \mathbb{R}^{3N}$, the equations of motion (57) can be recast in the equivalent form

$$\sum_{A,B=1}^{N} \delta\boldsymbol{q}_A \cdot \left(M^{AB}\ddot{\boldsymbol{q}}_A + \nabla_{\boldsymbol{q}_A} V(\boldsymbol{q}) - \boldsymbol{F}^A_{\text{ext}}(\boldsymbol{q}) \right) = 0 \tag{59}$$

for arbitrary $\delta \boldsymbol{q}_A \in \mathbb{R}^3$, $A = 1, \ldots, N$. Comparing (59) with (39) yields the mass matrix $\boldsymbol{M} \in \mathbb{R}^{3N \times 3N}$ pertaining to the Cosserat point

$$\boldsymbol{M} = \begin{bmatrix} M\boldsymbol{I} & \boldsymbol{0} & \boldsymbol{0} & \boldsymbol{0} \\ \boldsymbol{0} & E_0^{11}\boldsymbol{I} & E_0^{12}\boldsymbol{I} & E_0^{13}\boldsymbol{I} \\ \boldsymbol{0} & E_0^{21}\boldsymbol{I} & E_0^{22}\boldsymbol{I} & E_0^{23}\boldsymbol{I} \\ \boldsymbol{0} & E_0^{31}\boldsymbol{I} & E_0^{32}\boldsymbol{I} & E_0^{33}\boldsymbol{I} \end{bmatrix} \tag{60}$$

where $\boldsymbol{I}$ denotes the 3×3 identity matrix. Note that the mass matrix is constant, symmetric and positive-definite. In this connection we remark that, as is obvious from (27), $E_0^{ij} = E_0^{ji}$. Moreover, $V : \mathbb{R}^n \to \mathbb{R}$ is a potential energy function which, in the case of the Cosserat point, originates from the strain energy (13). In addition to the internal force vector $\boldsymbol{F}_{\text{int}}(\boldsymbol{q}) = \nabla V(\boldsymbol{q})$, the external force vector $\boldsymbol{F}_{\text{ext}}(\boldsymbol{q}) \in \mathbb{R}^n$ might represent configuration dependent (follower) loads. For the Cosserat point we have

$$\boldsymbol{F}_{\text{ext}} = \begin{bmatrix} \boldsymbol{F}^1_{\text{ext}} \\ \vdots \\ \boldsymbol{F}^N_{\text{ext}} \end{bmatrix} = \begin{bmatrix} \boldsymbol{f}_{\text{ext}} \\ \boldsymbol{f}^1_{\text{ext}} \\ \boldsymbol{f}^2_{\text{ext}} \\ \boldsymbol{f}^3_{\text{ext}} \end{bmatrix} \tag{61}$$

2.6.1 The 4-node Tetrahedral Element

One of the most frequently used low-order elements is the 4-node tetrahedral element and its two dimensional counterpart, the 3-node triangle. The present formulation of the Cosserat point is equivalent to the 4-node tetrahedral element (Fig. 3). Specifically, the configuration vector (58) of the Cosserat point, $\boldsymbol{q} \in \mathbb{R}^{12}$, can be directly connected to the four nodal position vectors, $\boldsymbol{x}_A \in \mathbb{R}^3$, $A \in \{1, 2, 3, 4\}$, characterizing the deformed configuration of the tetrahedral element. In view of the kinematic

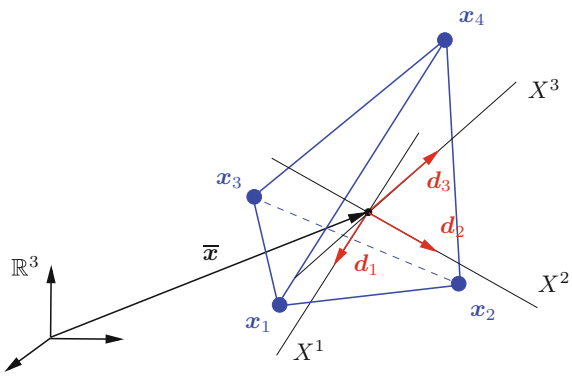

Fig. 3 The 4-node tetrahedral element and its connection with the Cosserat point

relationship (23), the nodal position vectors of the 4-node tetrahedral element can be expressed as

$$\boldsymbol{x}_A = \overline{\boldsymbol{x}} + X_A^i \, \boldsymbol{d}_i$$

where $\overline{\boldsymbol{x}} \in \mathbb{R}^3$ denotes the center of mass of the tetrahedral element and

$$X_A^i = \boldsymbol{D}^i \cdot (\boldsymbol{X}_A - \overline{\boldsymbol{X}})$$

are the material coordinates of the nodes in accordance with (22). We refer to Fig. 4 for an illustration of the planar case.

Introducing the nodal configuration vector of the 4-node tetrahedral element

$$\boldsymbol{q}^e = \left[\boldsymbol{x}_1^T \; \boldsymbol{x}_2^T \; \boldsymbol{x}_3^T \; \boldsymbol{x}_4^T\right]^T$$

we may write

$$\boldsymbol{q}^e = \boldsymbol{T}\boldsymbol{q}$$

where the configuration vector of the Cosserat point, $\boldsymbol{q} \in \mathbb{R}^{12}$ is given by (58), and $\boldsymbol{T}$ is a constant 12×12 transformation matrix of the form

$$\boldsymbol{T} = \begin{bmatrix} \boldsymbol{I} & X_1^1 \boldsymbol{I} & X_1^2 \boldsymbol{I} & X_1^3 \boldsymbol{I} \\ \boldsymbol{I} & X_2^1 \boldsymbol{I} & X_2^2 \boldsymbol{I} & X_2^3 \boldsymbol{I} \\ \boldsymbol{I} & X_3^1 \boldsymbol{I} & X_3^2 \boldsymbol{I} & X_3^3 \boldsymbol{I} \\ \boldsymbol{I} & X_4^1 \boldsymbol{I} & X_4^2 \boldsymbol{I} & X_4^3 \boldsymbol{I} \end{bmatrix}$$

For regular geometries of the tetrahedral element, matrix $\boldsymbol{T}$ is non-singular. Substituting the relationships

$$\boldsymbol{q} = \boldsymbol{T}^{-1}\boldsymbol{q}^e\,, \quad \delta\boldsymbol{q} = \boldsymbol{T}^{-1}\delta\boldsymbol{q}^e\,, \quad \ddot{\boldsymbol{q}} = \boldsymbol{T}^{-1}\ddot{\boldsymbol{q}}^e$$

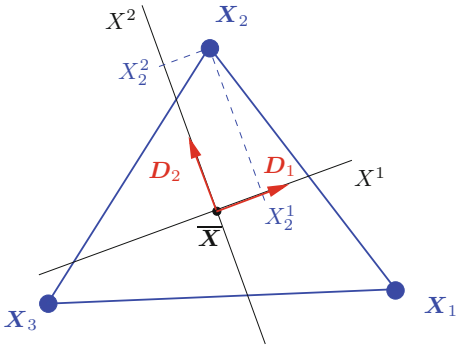

Fig. 4 The 3-node triangular element in the reference configuration. The position of node 2 relative to the center of mass, $\overline{\boldsymbol{X}} \in \mathbb{R}^2$, is characterized by the coordinates X_2^1 and X_2^2

into (59), the equations of motion can be written in terms of the nodal quantities pertaining to the tetrahedral element. For example, the corresponding mass matrix is given by

$$\boldsymbol{M}^e = \boldsymbol{T}^{-T}\boldsymbol{M}\boldsymbol{T}^{-1}$$

where the mass matrix $\boldsymbol{M}$ of the Cosserat point is given by (60).

2.7 The EM Method Due to Simo and Tarnow

We start our treatment of EM schemes by applying the method developed by Simo and Tarnow (1992) in the context of nonlinear elastodynamics to the model problem of an elastic Cosserat point. In essence the discretization in time of the ODEs (40) consists of a modification of the mid-point rule. Correspondingly, the resulting EM integrator is an implicit second-order scheme. For the present purposes it is convenient to confine our attention to the balances of director momentum $(40)_2$. Accordingly, we shall consider the following initial value problem written in first-order form: Find $\boldsymbol{d}_i, \boldsymbol{v}_i : [0, T] \to \mathbb{R}^3$, $(i = 1, 2, 3)$, such that

$$\begin{aligned} \dot{\boldsymbol{d}}_i &= \boldsymbol{v}_i \\ E_0^{ij}\dot{\boldsymbol{v}}_j &= \boldsymbol{f}^i_{\text{ext}} - \overline{S}^{ij}\boldsymbol{d}_j \end{aligned} \tag{62}$$

subject to the initial conditions $\boldsymbol{d}_i(0) = (\boldsymbol{d}_i)_0$, and $\boldsymbol{v}_i(0) = (\boldsymbol{v}_i)_0$, where $(\boldsymbol{d}_i)_0, (\boldsymbol{v}_i)_0 \in \mathbb{R}^3$ are given quantities. Note that expression (33) for the internal director forces, $\boldsymbol{f}^i_{\text{int}} = \overline{S}^{ij}\boldsymbol{d}_j$, has been used in $(62)_2$. Consider a representative time interval $[t_n, t_{n+1}]$ with time step $\Delta t = t_{n+1} - t_n$, and given state-space coordinates $\boldsymbol{d}_{i_n} \in \mathbb{R}^3$ and $\boldsymbol{v}_{i_n} \in \mathbb{R}^3$ at t_n. The resulting algebraic problem to be solved is given as follows: Find $(\boldsymbol{d}_{i_{n+1}}, \boldsymbol{v}_{i_{n+1}}) \in \mathbb{R}^3 \times \mathbb{R}^3$, $(i = 1, 2, 3)$, as the solution of the algebraic system of equations

$$\begin{aligned} \boldsymbol{d}_{i_{n+1}} - \boldsymbol{d}_{i_n} &= \Delta t \boldsymbol{v}_{i_{n+\frac{1}{2}}} \\ E_0^{ij}\big(\boldsymbol{v}_{j_{n+1}} - \boldsymbol{v}_{j_n}\big) &= \Delta t\big(\ (\boldsymbol{f}^i_{\text{ext}})\big|_{n+\frac{1}{2}} - \overline{S}^{ij}_A \boldsymbol{d}_{j_{n+\frac{1}{2}}}\big) \end{aligned} \tag{63}$$

Here and in the sequel $(\bullet)_{n+\frac{1}{2}}$ denotes the mean value of the quantity $(\bullet)$ in the time interval $[t_n, t_{n+1}]$. That is,

$$(\bullet)_{n+\frac{1}{2}} = \frac{1}{2}\big((\bullet)_n + (\bullet)_{n+1}\big) \tag{64}$$

Moreover, $(\boldsymbol{f}^i_{\text{ext}})\big|_{n+\frac{1}{2}}$ denotes the approximation of the external director forces in the time interval $[t_n, t_{n+1}]$, the specification of which is left open at the present stage. The distinguishing feature of the scheme (63) is the presence of an algorithmic stress formula for the calculation of $\overline{S}^{ij}_A$. In particular, for the specific case of *St. Venant-*

Kirchhoff material, in Simo and Tarnow (1992) the following closed-form expression for $\overline{S}_A^{ij}$ is proposed:

$$\overline{S}_A^{ij} = \mathsf{C}^{ijkl}\gamma_{kl_{n+\frac{1}{2}}} \tag{65}$$

Here, $\mathsf{C}^{ijkl} = 4\frac{\partial^2 U}{\partial d_{ij}\partial d_{kl}}$ are the components of the fourth-order elasticity tensor and γ_{ij} denote the components of the Green–Lagrangean strain tensor given by

$$\gamma_{ij} = \frac{1}{2}\left(d_{ij} - \delta_{ij}\right) \tag{66}$$

In view of (64) and (66), the algorithmic stress formula (65) relies on the mean value of the metric coefficients

$$\begin{aligned} d_{ij_{n+\frac{1}{2}}} &= \tfrac{1}{2}\left(d_{ij_n} + d_{ij_{n+1}}\right) \\ &= \tfrac{1}{2}\left(\boldsymbol{d}_{i_n}\cdot\boldsymbol{d}_{j_n} + \boldsymbol{d}_{i_{n+1}}\cdot\boldsymbol{d}_{j_{n+1}}\right) \end{aligned}$$

Note that this is in contrast to the mid-point rule, in which

$$\begin{aligned} d_{ij}^{\mathrm{MP}} &= \boldsymbol{d}_{i_{n+\frac{1}{2}}}\cdot\boldsymbol{d}_{j_{n+\frac{1}{2}}} \\ &= \tfrac{1}{2}d_{ij_{n+\frac{1}{2}}} + \tfrac{1}{4}\left(\boldsymbol{d}_{i_n}\cdot\boldsymbol{d}_{j_{n+1}} + \boldsymbol{d}_{i_{n+1}}\cdot\boldsymbol{d}_{j_n}\right) \\ &= d_{ij_{n+\frac{1}{2}}} - \tfrac{\Delta t^2}{4}\boldsymbol{v}_{i_{n+\frac{1}{2}}}\cdot\boldsymbol{v}_{j_{n+\frac{1}{2}}} \end{aligned} \tag{67}$$

would have to be used. In the last equation use has been made of $(63)_1$. We next show that the scheme is capable of conserving both angular momentum and energy.

2.7.1 Algorithmic Conservation of Angular Momentum

With regard to $(46)_1$ the angular momentum $\bar{\boldsymbol{j}}$ of the Cosserat point relative to its center of mass can be written in the form.

$$\bar{\boldsymbol{j}}(\boldsymbol{d}_i, \boldsymbol{v}_i) = E_0^{ij}\boldsymbol{d}_i \times \boldsymbol{v}_j \tag{68}$$

Obviously, the angular momentum is a quadratic function of the state-space coordinates $(\boldsymbol{d}_i, \boldsymbol{v}_i)$. To calculate the incremental change in the angular momentum we take into account the following remark.

Remark 2.5 When the map $f : \mathbb{R}^k \to \mathbb{R}$ is at most quadratic then the relationship

$$Df(\mathbf{y}_{n+\frac{1}{2}})\cdot(\mathbf{y}_{n+1} - \mathbf{y}_n) = f(\mathbf{y}_{n+1}) - f(\mathbf{y}_n) \tag{69}$$

holds.

Accordingly, setting $\boldsymbol{y} = (\boldsymbol{d}_1, \ldots, \boldsymbol{d}_3, \boldsymbol{v}_1, \ldots, \boldsymbol{v}_3)$, we get

$$\begin{aligned}
&\bar{\boldsymbol{j}}_{n+1} - \bar{\boldsymbol{j}}_n = \bar{\boldsymbol{j}}(\boldsymbol{y}_{n+1}) - \bar{\boldsymbol{j}}(\boldsymbol{y}_n) \\
&= \tfrac{\partial \bar{\boldsymbol{j}}}{\partial \boldsymbol{d}_i}(\boldsymbol{y}_{n+\frac{1}{2}})(\boldsymbol{d}_{i_{n+1}} - \boldsymbol{d}_{i_n}) + \tfrac{\partial \bar{\boldsymbol{j}}}{\partial \boldsymbol{v}_i}(\boldsymbol{y}_{n+\frac{1}{2}})(\boldsymbol{v}_{i_{n+1}} - \boldsymbol{v}_{i_n}) \\
&= -E_0^{ij}\widehat{\boldsymbol{v}}_{j_{n+\frac{1}{2}}}(\boldsymbol{d}_{i_{n+1}} - \boldsymbol{d}_{i_n}) + E_0^{ji}\widehat{\boldsymbol{d}}_{j_{n+\frac{1}{2}}}(\boldsymbol{v}_{i_{n+1}} - \boldsymbol{v}_{i_n})
\end{aligned}$$

Substituting form $(63)_1$ and $(63)_2$ into the last equation and taking into account the symmetry property $E_0^{ij} = E_0^{ji}$ yields

$$\begin{aligned}
\bar{\boldsymbol{j}}_{n+1} - \bar{\boldsymbol{j}}_n &= \widehat{\boldsymbol{d}}_{j_{n+\frac{1}{2}}} \Delta t \big((\boldsymbol{f}^j_{\text{ext}})\big|_{n+\frac{1}{2}} - \overline{S}_A^{ji} \boldsymbol{d}_{i_{n+\frac{1}{2}}} \big) \\
&= \Delta t \boldsymbol{d}_{j_{n+\frac{1}{2}}} \times (\boldsymbol{f}^j_{\text{ext}})\big|_{n+\frac{1}{2}} \\
&= \Delta t \, \overline{\boldsymbol{m}}_{\text{ext}}|_{n+\frac{1}{2}}
\end{aligned} \tag{70}$$

where the symmetry of $\overline{S}_A^{ji}$ has been accounted for. In the last equation $\overline{\boldsymbol{m}}_{\text{ext}}|_{n+\frac{1}{2}}$ denotes the discrete version of the resultant external torque relative to the center of mass defined by

$$\overline{\boldsymbol{m}}_{\text{ext}} = \boldsymbol{d}_i \times \boldsymbol{f}^i_{\text{ext}} \tag{71}$$

Note that this definition is in line with $(46)_2$. It is obvious from (70) that the present scheme conserves the angular momentum provided that the external torque vanishes.

2.7.2 Algorithmic Conservation of Energy

Combining $(63)_1$ and $(63)_2$ using the dot product leads to

$$\big(\boldsymbol{d}_{i_{n+1}} - \boldsymbol{d}_{i_n}\big) \cdot \big((\boldsymbol{f}^i_{\text{ext}})\big|_{n+\frac{1}{2}} - \overline{S}_A^{ij} \boldsymbol{d}_{j_{n+\frac{1}{2}}} \big) = \boldsymbol{v}_{i_{n+\frac{1}{2}}} \cdot E_0^{ij} \big(\boldsymbol{v}_{j_{n+1}} - \boldsymbol{v}_{j_n} \big) \tag{72}$$

Concerning the right-hand side of the last equation we get

$$\begin{aligned}
\boldsymbol{v}_{i_{n+\frac{1}{2}}} \cdot E_0^{ij} \big(\boldsymbol{v}_{j_{n+1}} - \boldsymbol{v}_{j_n} \big) &= \tfrac{1}{2} E_0^{ij} \big(\boldsymbol{v}_{i_{n+1}} \cdot \boldsymbol{v}_{j_{n+1}} - \boldsymbol{v}_{i_n} \cdot \boldsymbol{v}_{j_n} \big) \\
&= \overline{T}_{n+1} - \overline{T}_n
\end{aligned}$$

where the symmetry of E_0^{ij} has been taken into account. Moreover, $\overline{T}$ denotes the relative kinetic energy given by

$$\overline{T} = \frac{1}{2} E_0^{ij} \boldsymbol{v}_i \cdot \boldsymbol{v}_j \tag{73}$$

Note that the above expression for the relative kinetic energy is in line with definition (50) of the total kinetic energy of the Cosserat point. Furthermore,

$$\begin{aligned}\big(\boldsymbol{d}_{i_{n+1}}-\boldsymbol{d}_{i_n}\big)\cdot\overline{S}^{ij}_A\boldsymbol{d}_{j_{n+\frac{1}{2}}} &= \tfrac{1}{2}\overline{S}^{ij}_A\big(\boldsymbol{d}_{i_{n+1}}\cdot\boldsymbol{d}_{j_{n+1}}-\boldsymbol{d}_{i_n}\cdot\boldsymbol{d}_{j_n}\big)\\ &= \tfrac{1}{2}\overline{S}^{ij}_A\big(d_{ij_{n+1}}-d_{ij_n}\big)\\ &= \overline{S}^{ij}_A\big(\gamma_{ij_{n+1}}-\gamma_{ij_n}\big)\end{aligned}$$

where use has been made of the symmetry of $\overline{S}^{ij}_A$ along with the definition of the metric coefficients and the Green–Lagrangean strains (66). Employing the algorithmic stress formula (65), the last equation gives

$$\begin{aligned}\overline{S}^{ij}_A\big(\gamma_{ij_{n+1}}-\gamma_{ij_n}\big) &= \mathsf{C}^{ijkl}\gamma_{kl_{n+\frac{1}{2}}}\big(\gamma_{ij_{n+1}}-\gamma_{ij_n}\big)\\ &= \tfrac{1}{2}\big(\gamma_{ij_{n+1}}-\gamma_{ij_n}\big)\mathsf{C}^{ijkl}\big(\gamma_{kl_{n+1}}+\gamma_{kl_n}\big)\\ &= \tfrac{1}{2}\big(\gamma_{ij_{n+1}}\mathsf{C}^{ijkl}\gamma_{kl_{n+1}}-\gamma_{ij_n}\mathsf{C}^{ijkl}\gamma_{kl_n}\big)\end{aligned}$$

where the major symmetry $\mathsf{C}^{ijkl}=\mathsf{C}^{klij}$ of the elasticity tensor has been taken into account. The total strain energy of the St. Venant-Kirchhoff Cosserat point is given by

$$U^{\mathrm{St.V-K}}=\frac{1}{2}\gamma_{ij}\mathsf{C}^{ijkl}\gamma_{kl} \tag{74}$$

Altogether, Eq. (72) can be recast in the form

$$\begin{aligned}\Delta t\,\big(\boldsymbol{f}^i_{\mathrm{ext}}\big)\big|_{n+\frac{1}{2}}\,\boldsymbol{v}_{i_{n+\frac{1}{2}}} &= \overline{T}_{n+1}-\overline{T}_n+U^{\mathrm{St.V-K}}_{n+1}-U^{\mathrm{St.V-K}}_n\\ &= \overline{E}_{n+1}-\overline{E}_n\end{aligned} \tag{75}$$

where on the left-hand side of the last equation use has been made of $(63)_1$. Moreover, on the right-hand side the total energy $\overline{E}$ has been introduced, analogous to (49). The last equation corroborates algorithmic conservation of energy in the absence of external loading.

Remark 2.6 The above investigation shows that in order to achieve algorithmic conservation of energy the stress formula has to satisfy the condition

$$U_{n+1}-U_n=\frac{1}{2}\overline{S}^{ij}_A\big(d_{ij_{n+1}}-d_{ij_n}\big) \tag{76}$$

This condition can be viewed as discrete counterpart of

$$\frac{d}{dt}\tilde{U}(d_{ij})=\frac{\partial\tilde{U}}{\partial d_{ij}}\dot{d}_{ij}=\frac{1}{2}\overline{S}^{ij}\dot{d}_{ij}$$

In the last equation use has been made of (31).

Remark 2.7 The nonlinear system of equations emanating from the EM scheme (63) is typically solved iteratively by applying Newton's method. As outlined in Appendix A.3, the corresponding iteration matrix is nonsymmetric. This is in contrast to standard schemes such as the mid-point rule which yield a symmetric iteration matrix. This is the price one has to pay for the improved numerical stability of the EM integrator.

2.8 The Discrete Derivative

The closed-form expression for the algorithmic stress formula (65) proposed by Simo and Tarnow (1992) is restricted to St. Venant-Kirchhoff material. A generalized procedure for the design of second-order EM integrators relies on the notation of a discrete derivative introduced in Gonzalez (1996). This approach makes possible the design of appropriate algorithmic stress formulas for general hyperelastic constitutive laws. Moreover, symmetries of the mechanical system can be taken into account by the introduction of specific invariants. If the invariants and the corresponding momentum maps are *at most quadratic*, the resulting time-stepping scheme is capable of conserving the respective momentum map. As has been shown above the momentum map of primary interest in the present work is the total angular momentum. In this connection the metric coefficients play the role of quadratic invariants (see Remark 2.4). In analogy to (35), see Remark 2.1, the discrete version of the derivative $\partial \hat{U}/\partial \boldsymbol{d}_i$ is chosen to be

$$\overline{\nabla}_{d_i} U(\boldsymbol{d}_{j_n}, \boldsymbol{d}_{j_{n+1}}) = \mathsf{D}\tilde{U}(d_{jk_n}, d_{jk_{n+1}}) \frac{\partial d_{jk}}{\partial \boldsymbol{d}_i}(\boldsymbol{d}_{l_{n+\frac{1}{2}}}) \tag{77}$$

where

$$\mathsf{D}\tilde{U}(d_{ik_n}, d_{ik_{n+1}}) = \mathsf{S}^{ik} + \frac{U_{n+1} - U_n - \mathsf{S}^{jl}\Delta d_{jl}}{\Delta d_{mn}\Delta d_{mn}} \Delta d_{ik} \tag{78}$$

with

$$\mathsf{S}^{ik} = D\tilde{U}(d_{ik_{n+\frac{1}{2}}}) \qquad \text{and} \qquad \Delta d_{ik} = d_{ik_{n+1}} - d_{ik_n}$$

Similar to (35), the discrete gradient (77) can be written as

$$\overline{\nabla}_{d_i} U(\boldsymbol{d}_{j_n}, \boldsymbol{d}_{j_{n+1}}) = 2\mathsf{D}\tilde{U}(d_{ik_n}, d_{ik_{n+1}}) \boldsymbol{d}_{k_{n+\frac{1}{2}}} \tag{79}$$

Using the discrete gradient (77), the EM scheme (63) can be recast in the form

$$\begin{aligned} \boldsymbol{d}_{i_{n+1}} - \boldsymbol{d}_{i_n} &= \Delta t \boldsymbol{v}_{i_{n+\frac{1}{2}}} \\ E_0^{ij}\big(\boldsymbol{v}_{j_{n+1}} - \boldsymbol{v}_{j_n}\big) &= \Delta t\big((\boldsymbol{f}_{\text{ext}}^i)\big|_{n+\frac{1}{2}} - \overline{\nabla}_{d_i} U(\boldsymbol{d}_{j_n}, \boldsymbol{d}_{j_{n+1}})\big) \end{aligned} \tag{80}$$

We refer to this scheme as the *EM integrator for hyperelastic Cosserat points*. In the present context the discrete gradient (79) gives rise to the algorithmic stress formula

$$\overline{S}_A^{ij} = 2\mathsf{D}\tilde{U}(d_{ij_n}, d_{ij_{n+1}}) \tag{81}$$

2.8.1 Directionality Property of the Discrete Derivative

In analogy to the following continuous relationship

$$\frac{d}{dt}U = \frac{\partial \hat{U}}{\partial \boldsymbol{d}_k} \cdot \dot{\boldsymbol{d}}_k$$

the discrete derivative satisfies by design the so-called directionality property (Gonzalez 1996)

$$U_{n+1} - U_n = \overline{\nabla}_{d_i} U \cdot \left(\boldsymbol{d}_{i_{n+1}} - \boldsymbol{d}_{i_{n+1}}\right) \tag{82}$$

To see this, substitute from (77) into the last equation to get

$$\begin{aligned} U_{n+1} - U_n &= \mathsf{D}\tilde{U}(d_{jk_n}, d_{jk_{n+1}}) \frac{\partial d_{jk}}{\partial \boldsymbol{d}_i}(\boldsymbol{d}_{l_{n+\frac{1}{2}}}) \cdot \left(\boldsymbol{d}_{i_{n+1}} - \boldsymbol{d}_{i_{n+1}}\right) \\ &= \mathsf{D}\tilde{U}(d_{jk_n}, d_{jk_{n+1}})\left(d_{jk_{n+1}} - d_{jk_n}\right) \end{aligned} \tag{83}$$

Here Remark 2.5 has been applied since the metric coefficients d_{jk} are merely quadratic functions of $\boldsymbol{d}_i$. It can be easily verified that formula (78) satisfies the last equation by design.

2.8.2 Algorithmic Conservation Properties

Due to the directionality property $(83)_2$ the algorithmic stress formula (81) automatically fulfills the condition (76) for the conservation of energy. Moreover, the above proof of algorithmic conservation of angular momentum remains unaltered.

Remark 2.8 Condition (76) for algorithmic energy conservation can be used as algebraic constraint in an optimization problem to devise suitable stress formulas for second-order EM schemes, see Groß et al. (2005, Sect. 6.8) and Romero (2012). In particular, in these works, formula (78) is derived by applying the optimization approach. Moreover, the optimization approach is employed in the Galerkin-based discretization method in Groß et al. (2005, Sect. 6) to construct higher-order EM schemes for nonlinear elastodynamics.

Remark 2.9 While the notion of a discrete derivative makes possible the design of EM schemes for general hyperelastic constitutive laws, stress formula (81) boils down to (65) in the case of the St. Venant-Kirchhoff model. This can be shown by

inserting the total strain energy (74) pertaining to the St. Venant-Kirchhoff model into the discrete derivative (78).

Remark 2.10 The discrete derivative of a quadratic function coincides with the standard derivative evaluated at $(\bullet)_{n+\frac{1}{2}}$. In particular, since the strain energy of the St. Venant-Kirchhoff model is merely a quadratic function of the metric coefficients or Green–Lagrangean strains, respectively, the discrete derivative (81) coincides with the standard derivative

$$\begin{aligned} \overline{S}_A^{ij} &= 2D\tilde{U}^{\mathrm{St.V-K}}\left(d_{ij_{n+\frac{1}{2}}}\right) \\ &= D\tilde{U}^{\mathrm{St.V-K}}\left(\gamma_{ij_{n+\frac{1}{2}}}\right) \\ &= \mathsf{C}^{ijkl}\gamma_{kl_{n+\frac{1}{2}}} \end{aligned} \tag{84}$$

where relation (66) between the metric coefficients d_{ij} and the Green–Lagrangean strains γ_{ij} has been taken into account along with the strain energy function (74). This result is in agreement with stress formula (65) due to Simo and Tarnow (1992), and therefore complements Remark 2.9.

Remark 2.11 In the *linearized theory* the strains are merely linear functions of the displacements. In the present context the linearized strains are given by

$$\gamma_{ij}^{\mathrm{lin}} = \frac{1}{2}\left(\boldsymbol{u}_i \cdot \boldsymbol{D}_j + \boldsymbol{D}_i \cdot \boldsymbol{u}_j\right)$$

Note that the director displacements $\boldsymbol{u}_i \in \mathbb{R}^3$ have been introduced such that the relationship $\boldsymbol{d}_i = \boldsymbol{D}_i + \boldsymbol{u}_i$ holds. The strain energy (74) thus becomes a quadratic function of the displacements and can be written as

$$U_{\mathrm{lin}} = \frac{1}{2}\boldsymbol{u}_i \cdot \boldsymbol{K}^{ij}\boldsymbol{u}_j$$

where $\boldsymbol{K}^{ij} \in \mathbb{R}^{3\times 3}$ constitutes a symmetric stiffness matrix. Consequently, due to the properties of the discrete derivative (cf. Remark 2.10),

$$\begin{aligned} \overline{\nabla}_{d_i} U_{\mathrm{lin}}(\boldsymbol{d}_{j_n}, \boldsymbol{d}_{j_{n+1}}) &= \nabla U_{\mathrm{lin}}(\boldsymbol{d}_{j_{n+\frac{1}{2}}}) \\ &= \tfrac{1}{2}\left(\nabla U_{\mathrm{lin}}(\boldsymbol{d}_{j_n}) + \nabla U_{\mathrm{lin}}(\boldsymbol{d}_{j_{n+1}})\right) \\ &= \tfrac{1}{2}\boldsymbol{K}^{ij}\left(\boldsymbol{u}_{j_n} + \boldsymbol{u}_{j_{n+1}}\right)) \end{aligned}$$

Accordingly, for linear problems the EM integrator (80) coincides with the trapezoidal rule (or average acceleration method) which is a member of the Newmark family, see Hughes (2000). The average acceleration method is known to be energy preserving, unconditionally stable, and one of the most widely used methods for structural dynamics applications.

3 Rigid Body Dynamics

3.1 From the Cosserat Point to the Rigid Body

We next perform the transition from the theory of a Cosserat point to rigid body dynamics (Fig. 5). To this end we consider the imposition of geometric constraints on the Cosserat point. In particular, the constraints can be included in a straightforward way by replacing the strain energy (13) with an augmented potential function

$$V_\lambda(\boldsymbol{d}_i) = \hat{U}(\boldsymbol{d}_i) + \sum_{l=1}^{R} \lambda^l \hat{g}_l(\boldsymbol{d}_i) \tag{85}$$

Here, $\lambda^l : [0, T] \to \mathbb{R}$ are Lagrange multipliers for the enforcement of the (holonomic) constraints $g_l = 0$. Similar to the strain energy (52), frame-indifferent constraint functions are given by

$$g_l = \hat{g}_l(\boldsymbol{d}_i) = \tilde{g}_l(d_{ij}) \tag{86}$$

For example, the constraint $g_1 = \boldsymbol{d}_1 \cdot \boldsymbol{d}_1 - 1 = 0$ eliminates extension in the direction of $\boldsymbol{d}_1$. For a rigid body we have to impose $R = 6$ independent constraints. To this end we choose (85) to be of the form

$$\begin{aligned} V_\lambda^{\mathrm{RB}} = \sum_{l=1}^{6} \lambda^l \tilde{g}_l(d_{ij}) &= \boldsymbol{\Lambda} : \tfrac{1}{2}(\boldsymbol{C} - \boldsymbol{I}) \\ &= \boldsymbol{\Lambda} : \tfrac{1}{2}\big((d_{ij} - \delta_{ij})\boldsymbol{D}^i \otimes \boldsymbol{D}^j\big) \\ &= \boldsymbol{D}^i \cdot \boldsymbol{\Lambda}\boldsymbol{D}^j \tfrac{1}{2}(d_{ij} - \delta_{ij}) \\ &= \Lambda^{ij} \tfrac{1}{2}(d_{ij} - \delta_{ij}) \end{aligned} \tag{87}$$

Here, the Lagrange multipliers are contained in the symmetric tensor $\boldsymbol{\Lambda}$ according to the following assignment

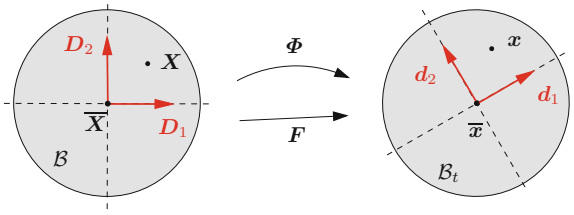

Fig. 5 Planar illustration of the transition from the elastic Cosserat point to the rigid body: The director frame $\{\boldsymbol{d}_i\}$ is forced to stay orthonormal for all time. Correspondingly, $\boldsymbol{F} \in \mathrm{SO}(3)$, see Remark 3.1

$$\begin{bmatrix} \lambda^1 \\ \lambda^2 \\ \lambda^3 \\ \lambda^4 \\ \lambda^5 \\ \lambda^6 \end{bmatrix} = \begin{bmatrix} \Lambda^{11} \\ \Lambda^{22} \\ \Lambda^{33} \\ \Lambda^{12} \\ \Lambda^{13} \\ \Lambda^{23} \end{bmatrix} \tag{88}$$

giving rise to the following six independent constraints of rigidity:

$$[\tilde{g}_l(d_{ij})] = \begin{bmatrix} \frac{1}{2}(d_{11} - 1) \\ \frac{1}{2}(d_{22} - 1) \\ \frac{1}{2}(d_{33} - 1) \\ d_{12} \\ d_{13} \\ d_{23} \end{bmatrix} = \mathbf{0} \tag{89}$$

As before (see Sect. 2.2), we assume that the director triad $\{\boldsymbol{D}_i\}$ in the reference configuration is orthonormal, that is, $\boldsymbol{D}_i \cdot \boldsymbol{D}_j = \delta_{ij}$. Accordingly, the constraints $\tilde{g}_l(\delta_{ij}) = 0$ $(l = 1, \ldots, 6)$ are identically fulfilled in the reference configuration. Imposing these constraints forces the director triad $\{\boldsymbol{d}_i(t)\}$ to stay orthonormal for all time. The configuration space corresponding to the motion of the rigid body about its center of mass is given by

$$\mathsf{Q} = \{\boldsymbol{d}_i \in \mathbb{R}^3 \mid \tilde{g}_l(d_{ij}) = 0\,,\ 1 \le l \le 6\,, (\boldsymbol{d}_1 \times \boldsymbol{d}_2) \cdot \boldsymbol{d}_3 = 1\} \tag{90}$$

Accordingly, the nine director components are subject to six independent constraints of rigidity. This is in agreement with the fact that the rotational motion of a rigid body has three degrees of freedom. The director velocities $\boldsymbol{v}_i$ have to belong to the tangent space to Q at $\boldsymbol{d}_i \in \mathsf{Q}$ given by

$$T_{d_i}\mathsf{Q} = \{\boldsymbol{v}_i \in \mathbb{R}^3 \mid \boldsymbol{v}_i = \boldsymbol{\omega} \times \boldsymbol{d}_i\,, \boldsymbol{\omega} \in \mathbb{R}^3\} \tag{91}$$

where $\boldsymbol{\omega}$ is the angular velocity (Fig. 6). It can be easily verified that the director velocities $\boldsymbol{v}_i \in T_{d_i}\mathsf{Q}$ satisfy the constraints on the velocity level given by

$$\frac{d}{dt}\left(\frac{1}{2}\big(d_{ij} - \delta_{ij}\big)\right) = \frac{1}{2}\big(\boldsymbol{d}_i \cdot \boldsymbol{v}_j + \boldsymbol{v}_i \cdot \boldsymbol{d}_j\big) = 0 \tag{92}$$

The equations governing the rotational motion of the free rigid body can be easily deduced from the Cosserat point by replacing the internal director forces

$$\boldsymbol{f}^i_{\text{int}} = \frac{\partial U}{\partial \boldsymbol{d}_i} = 2\frac{\partial U}{\partial d_{ik}}\boldsymbol{d}_k = \overline{S}^{ik}\boldsymbol{d}_k \tag{93}$$

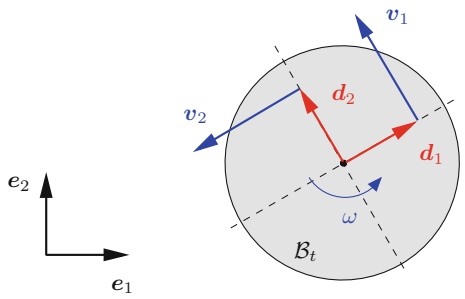

Fig. 6 Planar illustration of the rotation of a rigid body with angular velocity $\boldsymbol{\omega} = \omega \boldsymbol{e}_3$ and director velocities $\boldsymbol{v}_i \in T_{d_i}\mathsf{Q}$

with the constraint director forces

$$\boldsymbol{f}_{\mathrm{c}}^{i} = \frac{\partial V_{\lambda}^{\mathrm{RB}}}{\partial \boldsymbol{d}_i} = \sum_{l=1}^{6} \lambda^l \frac{\partial g_l}{\partial \boldsymbol{d}_i} = 2 \frac{\partial V_{\lambda}^{\mathrm{RB}}}{\partial d_{ik}} \boldsymbol{d}_k = \Lambda^{ik} \boldsymbol{d}_k \tag{94}$$

Here, Remark 2.1 along with (87) have been taken into account. Now the initial value problem governing the rotational motion of the rigid body can be directly deduced from the corresponding problem pertaining to the Cosserat point (see Sect. 2.7): Find $(\boldsymbol{d}_i, \boldsymbol{v}_i) \in \mathbb{R}^3 \times \mathbb{R}^3$ $(i = 1, 2, 3)$, and $\lambda_l \in \mathbb{R}$ $(l = 1, \ldots, 6)$, such that

$$\begin{aligned} \dot{\boldsymbol{d}}_i &= \boldsymbol{v}_i \\ E_0^{ij} \dot{\boldsymbol{v}}_j &= \boldsymbol{f}_{\mathrm{ext}}^{i} - \Lambda^{ij} \boldsymbol{d}_j \\ \hat{g}_l(\boldsymbol{d}_i) &= 0 \end{aligned} \tag{95}$$

subject to the initial conditions $\boldsymbol{d}_i(0) = (\boldsymbol{d}_i)_0$, and $\boldsymbol{v}_i(0) = (\boldsymbol{v}_i)_0$, where $(\boldsymbol{d}_i)_0 \in \mathsf{Q}$, and $(\boldsymbol{v}_i)_0 \in T_{d_i}\mathsf{Q}$ are given quantities. While the motion of the hyperelastic Cosserat point is governed by ODEs, the present rigid body formulation relies on differential-algebraic equations (DAEs). As is common with constrained mechanical systems the DAEs (95) have (differential) index three. For more background on DAEs we refer to Ascher and Petzold (1998) and Kunkel and Mehrmann (2006). Note that the constraints $(95)_3$ provide six algebraic equations for the determination of the six independent Lagrange multipliers (88). In contrast to that, the six stress resultants $\overline{S}^{ij}$ of the hyperelastic Cosserat point are depending on the Green–Lagrangean strains (or metric coefficients) via the constitutive law.

Remark 3.1 Imposition of the six independent constraints of rigidity (89) is equivalent to the enforcement of zero Green–Lagrangean strains, that is $\gamma_{ij} = 0$, or

$$\boldsymbol{G} = \frac{1}{2}(\boldsymbol{C} - \boldsymbol{I}) = \gamma_{ij} \boldsymbol{D}^i \otimes \boldsymbol{D}^j = \boldsymbol{0}$$

The last equation implies

$$\boldsymbol{C} = \boldsymbol{F}^T \boldsymbol{F} = \boldsymbol{I}$$

Taking into account the original requirement $\det(\boldsymbol{F}) > 0$ for the Cosserat point, the last equation yields

$$\boldsymbol{F}^T\boldsymbol{F} = \boldsymbol{I} \qquad \text{and} \qquad \det(\boldsymbol{F}) = 1$$

Consequently, in the case of the rigid body, the deformation gradient coincides with a rotation tensor $\boldsymbol{F} \in \mathrm{SO}(3)$.

3.2 Balance of Angular Momentum

For the free rigid body, balance of angular momentum can be shown along the lines of the previous treatment of the Cosserat point. In particular, the balance law (45) together with the definition of the angular momentum and the resultant external torque in (46) remain unaltered. Accordingly, scalar multiplying $(95)_2$ by $\boldsymbol{\xi} \times \boldsymbol{d}_i$ yields

$$(\boldsymbol{\xi} \times \boldsymbol{d}_i) \cdot E_0^{ij}\dot{\boldsymbol{v}}_j = (\boldsymbol{\xi} \times \boldsymbol{d}_i) \cdot (\boldsymbol{f}^i_{\text{ext}} - \Lambda^{ij}\boldsymbol{d}_j)$$

or

$$\boldsymbol{\xi} \cdot \left(E_0^{ij}\boldsymbol{d}_i \times \dot{\boldsymbol{v}}_j - \boldsymbol{d}_i \times \boldsymbol{f}^i_{\text{ext}} + \Lambda^{ij}\boldsymbol{d}_i \times \boldsymbol{d}_j\right) = 0$$

Due to the symmetry of Λ^{ij} the constraint director forces drop out of the last equation. The fact that the constraint director forces (94) do not contribute to the balance of angular momentum can be linked to the rotational invariance of the function $V_\lambda^{\mathrm{RB}} : \mathsf{Q} \to \mathbb{R}$. This is in complete analogy to Remark 2.3. Due to the arbitrariness of $\boldsymbol{\xi} \in \mathbb{R}^3$, the last equation yields the balance of angular momentum

$$\begin{aligned} \frac{d}{dt}\left(E_0^{ij}\boldsymbol{d}_i \times \boldsymbol{v}_j\right) &= \boldsymbol{d}_i \times \boldsymbol{f}^i_{\text{ext}} \\ \frac{d}{dt}\bar{\boldsymbol{j}} &= \overline{\boldsymbol{m}}_{\text{ext}} \end{aligned} \tag{96}$$

relative to the center of mass of the rigid body. Note that the quantities $\bar{\boldsymbol{j}}$ and $\overline{\boldsymbol{m}}_{\text{ext}}$ have been introduced before in (68) and (71), respectively.

3.3 Balance of Energy

Balance of energy can be shown for the rigid body along the lines of the previous treatment of the Cosserat point. Accordingly, scalar multiplying $(95)_2$ by $\boldsymbol{v}_i$ yields

$$\boldsymbol{v}_i \cdot \left(E_0^{ij}\dot{\boldsymbol{v}}_j - \boldsymbol{f}^i_{\text{ext}} + \Lambda^{ij}\boldsymbol{d}_j\right) = 0 \tag{97}$$

Due to the symmetry of Λ^{ij} the rate of work done by the constraint director forces (94) can be written as

$$\begin{aligned} \boldsymbol{f}^i_{\mathrm{c}} \cdot \boldsymbol{v}_i &= \Lambda^{ij} \boldsymbol{d}_j \cdot \boldsymbol{v}_i \\ &= \Lambda^{ij} \tfrac{1}{2} (\boldsymbol{d}_i \cdot \boldsymbol{v}_j + \boldsymbol{d}_j \cdot \boldsymbol{v}_i) \\ &= 0 \end{aligned}$$

The last equality holds due to the constraints on the velocity level (92). This property complies with the fact that ideal forces of constraint are workless. Finally, (97) can be recast in the form

$$\frac{d}{dt} \left(\frac{1}{2} E^{ij}_0 \boldsymbol{v}_i \cdot \boldsymbol{v}_j \right) = \boldsymbol{f}^i_{\mathrm{ext}} \cdot \boldsymbol{v}_i$$

This is the balance of energy for the rotational motion of the rigid body about its center of mass. The last equation can also be written as $\frac{d}{dt} \overline{T} = \overline{P}_{\mathrm{ext}}$, where $\overline{T}$ denotes the relative kinetic energy introduced in (73) and

$$\overline{P}_{\mathrm{ext}} = \boldsymbol{f}^i_{\mathrm{ext}} \cdot \boldsymbol{v}_i \tag{98}$$

denotes the power of the external director forces. Note that the quantities $\overline{T}$ and (98) correspond to the quantities (50) and (48), respectively, in the previous treatment of the Cosserat point.

3.4 Connection with the Classical Euler's Equations

We next link the present equations for the rotational motion of the rigid body to the classical Euler's equations. To this end we recast $(95)_2$ in the form

$$\delta \boldsymbol{d}_i \cdot \left(E^{ij}_0 \dot{\boldsymbol{v}}_j - \boldsymbol{f}^i_{\mathrm{ext}} + \Lambda^{ij} \boldsymbol{d}_j \right) = 0 \tag{99}$$

which has to hold for arbitrary $\delta \boldsymbol{d}_i \in \mathbb{R}^3$. Now we impose $\delta \boldsymbol{d}_i \in T_{d_i} \mathsf{Q}$. With regard to (91), we set $\delta \boldsymbol{d}_i = \delta \boldsymbol{\vartheta} \times \boldsymbol{d}_i$ for any $\delta \boldsymbol{\vartheta} \in \mathbb{R}^3$ such that (99) can be rewritten as

$$\delta \boldsymbol{\vartheta} \cdot \left(E^{ij}_0 \boldsymbol{d}_i \times \dot{\boldsymbol{v}}_j - \boldsymbol{d}_i \times \boldsymbol{f}^i_{\mathrm{ext}} \right) = 0$$

Note that in analogy to Sect. 3.2 the constraint director forces drop out of the last equation. The last equation can also be written as

$$E^{ij}_0 \boldsymbol{d}_i \times \dot{\boldsymbol{v}}_j = \overline{\boldsymbol{m}}_{\mathrm{ext}} \tag{100}$$

where $\overline{\boldsymbol{m}}_{\text{ext}}$ denotes the resultant external torque relative to the center of mass (see (71)). We next introduce the angular velocity $\boldsymbol{\omega} \in \mathbb{R}^3$ to confine the director velocities to $\boldsymbol{v}_i \in T_{d_i}\mathsf{Q}$. Accordingly, we have $\boldsymbol{v}_i = \boldsymbol{\omega} \times \boldsymbol{d}_i$ such that

$$\begin{aligned} \dot{\boldsymbol{v}}_j &= \dot{\boldsymbol{\omega}} \times \boldsymbol{d}_j + \boldsymbol{\omega} \times \boldsymbol{v}_j \\ &= \dot{\boldsymbol{\omega}} \times \boldsymbol{d}_j + \boldsymbol{\omega} \times (\boldsymbol{\omega} \times \boldsymbol{d}_j) \end{aligned}$$

Now the left-hand side of (100) can be written as

$$\begin{aligned} E_0^{ij} \boldsymbol{d}_i \times \dot{\boldsymbol{v}}_j &= E_0^{ij} \boldsymbol{d}_i \times (\dot{\boldsymbol{\omega}} \times \boldsymbol{d}_j) + E_0^{ij} \boldsymbol{d}_i \times (\boldsymbol{\omega} \times (\boldsymbol{\omega} \times \boldsymbol{d}_j)) \\ &= E_0^{ij} \boldsymbol{d}_i \times (\dot{\boldsymbol{\omega}} \times \boldsymbol{d}_j) + \boldsymbol{\omega} \times (E_0^{ij} \boldsymbol{d}_i \times (\boldsymbol{\omega} \times \boldsymbol{d}_j)) \end{aligned} \tag{101}$$

The last equality can be verified by a straightforward calculation using the properties of the vector triple product along with the symmetry of E_0^{ij}. Next consider

$$\begin{aligned} E_0^{ij} \boldsymbol{d}_i \times (\boldsymbol{a} \times \boldsymbol{d}_j) &= E_0^{ij} [(\boldsymbol{d}_i \cdot \boldsymbol{d}_j)\boldsymbol{a} - (\boldsymbol{d}_i \cdot \boldsymbol{a})\boldsymbol{d}_j] \\ &= E_0^{ij} [\delta_{ij} \boldsymbol{I} - \boldsymbol{d}_j \otimes \boldsymbol{d}_i]\boldsymbol{a} \\ &= [\text{tr}(\boldsymbol{E})\boldsymbol{I} - \boldsymbol{E}]\boldsymbol{a} \\ &= \boldsymbol{J}\boldsymbol{a} \end{aligned} \tag{102}$$

for any $\boldsymbol{a} \in \mathbb{R}^3$. Here, the current Euler tensor

$$\boldsymbol{E} = \boldsymbol{F}\boldsymbol{E}_0\boldsymbol{F}^T = E_0^{ij} \boldsymbol{d}_i \otimes \boldsymbol{d}_j$$

has been introduced. Note that $\boldsymbol{E}$ has the same coefficients as the referential Euler tensor (9). Moreover, in (102) the rigid body constraints, namely $d_{ij} = \delta_{ij}$, have been taken into account. Eventually, the classical inertia tensor

$$\boldsymbol{J} = \text{tr}(\boldsymbol{E})\boldsymbol{I} - \boldsymbol{E}$$

has been introduced. Now we are in a position to recast (100) in the form

$$\boldsymbol{J}\dot{\boldsymbol{\omega}} + \boldsymbol{\omega} \times \boldsymbol{J}\boldsymbol{\omega} = \overline{\boldsymbol{m}}_{\text{ext}}$$

which corresponds to the classical Euler's equations for the rigid body.

3.5 EM Integrator for the Rigid Body

As has been shown above, the equations of motion for the rigid body can be directly deduced from those for the hyperelastic Cosserat point by replacing the strain energy (13) with the augmented potential function (87). To construct an EM scheme we apply the notion of a discrete derivative to the new potential function (87). That is,

in analogy to the continuous formulation (94), the discrete version of the constraint director forces is given by

$$\begin{aligned}(\boldsymbol{f}^i_{\mathrm{c}})\big|_{n+\frac{1}{2}} &= \overline{\nabla}_{d_i} V^{\mathrm{RB}}_{\lambda}(\boldsymbol{d}_{j_n}, \boldsymbol{d}_{j_{n+1}}) \\ &= \sum_{l=1}^{6} \lambda^l \overline{\nabla}_{d_i} g_l(\boldsymbol{d}_{j_n}, \boldsymbol{d}_{j_{n+1}}) \\ &= 2\mathsf{D}\tilde{V}^{\mathrm{RB}}_{\lambda}(d_{ik_n}, d_{ik_{n+1}})\boldsymbol{d}_{k_{n+\frac{1}{2}}} \\ &= \Lambda^{ik}\boldsymbol{d}_{k_{n+\frac{1}{2}}}\end{aligned} \tag{103}$$

Now the rigid body variant of the EM scheme (80) for the hyperelastic Cosserat point can be written as follows. Given $\boldsymbol{d}_{i_n} \in \mathsf{Q}$ and $\boldsymbol{v}_{i_n} \in \mathbb{R}^3$, $(i = 1, 2, 3)$, find $(\boldsymbol{d}_{i_{n+1}}, \boldsymbol{v}_{i_{n+1}}) \in \mathbb{R}^3 \times \mathbb{R}^3$, and $\lambda_{l_{n+1}} \in \mathbb{R}$ $(l = 1, \ldots, 6)$, as the solution of the algebraic system of equations

$$\begin{aligned}\boldsymbol{d}_{i_{n+1}} - \boldsymbol{d}_{i_n} &= \Delta t \boldsymbol{v}_{i_{n+\frac{1}{2}}} \\ E^{ij}_0\big(\boldsymbol{v}_{j_{n+1}} - \boldsymbol{v}_{j_n}\big) &= \Delta t\big((\boldsymbol{f}^i_{\mathrm{ext}})\big|_{n+\frac{1}{2}} - \Lambda^{ij}_{n+1}\boldsymbol{d}_{j_{n+\frac{1}{2}}}\big) \\ \hat{g}_l(\boldsymbol{d}_{i_{n+1}}) &= 0\end{aligned} \tag{104}$$

The scheme (104) provides 24 algebraic equations for the determination of the 18 state space coordinates $(\boldsymbol{d}_{i_{n+1}}, \boldsymbol{v}_{i_{n+1}})$ and the 6 independent Lagrange multipliers in Λ^{ij}_{n+1}. We further remark that $(104)_3$ ensures that $\boldsymbol{d}_{i_{n+1}} \in \mathsf{Q}$.

3.5.1 Algorithmic Conservation of Energy

This can be shown as before (see Sect. 2.7.2). One just has to replace the stress resultants $\overline{S}^{ij}_A$ with the Lagrange multipliers Λ^{ij}_{n+1}. Accordingly, combining $(104)_1$ and $(104)_2$ using the dot product yields

$$\big(\boldsymbol{d}_{i_{n+1}} - \boldsymbol{d}_{i_n}\big) \cdot \big((\boldsymbol{f}^i_{\mathrm{ext}})\big|_{n+\frac{1}{2}} - \Lambda^{ij}_{n+1}\boldsymbol{d}_{j_{n+\frac{1}{2}}}\big) = \boldsymbol{v}_{i_{n+\frac{1}{2}}} \cdot E^{ij}_0\big(\boldsymbol{v}_{j_{n+1}} - \boldsymbol{v}_{j_n}\big)$$

or

$$\Delta t\ (\boldsymbol{f}^i_{\mathrm{ext}})\big|_{n+\frac{1}{2}} \cdot \boldsymbol{v}_{i_{n+\frac{1}{2}}} - \big(\boldsymbol{d}_{i_{n+1}} - \boldsymbol{d}_{i_n}\big) \cdot (\boldsymbol{f}^i_{\mathrm{c}})\big|_{n+\frac{1}{2}} = \overline{T}_{n+1} - \overline{T}_n \tag{105}$$

On the right-hand side of the last equation the relative kinetic energy $\overline{T}$ (see (73)) has been introduced. On the left-hand side the discrete constraint director forces (103) have been used. Now consider

$$\begin{aligned}\big(\boldsymbol{d}_{i_{n+1}} - \boldsymbol{d}_{i_n}\big) \cdot (\boldsymbol{f}^i_{\mathrm{c}})\big|_{n+\frac{1}{2}} &= \sum_{l=1}^{6} \lambda^l_{n+1} \overline{\nabla}_{d_i} g_l(\boldsymbol{d}_{j_n}, \boldsymbol{d}_{j_{n+1}}) \cdot \big(\boldsymbol{d}_{i_{n+1}} - \boldsymbol{d}_{i_n}\big) \\ &= \sum_{l=1}^{6} \lambda^l_{n+1}\big(\hat{g}_l(\boldsymbol{d}_{j_{n+1}}) - \hat{g}_l(\boldsymbol{d}_{j_n})\big) \\ &= 0\end{aligned} \tag{106}$$

In the last equation use has been made of the directionality property of the discrete derivative, see (82). In the present context we have

$$\hat{g}_l(\boldsymbol{d}_{j_{n+1}}) - \hat{g}_l(\boldsymbol{d}_{j_n}) = \overline{\nabla}_{d_i} g_l(\boldsymbol{d}_{j_n}, \boldsymbol{d}_{j_{n+1}}) \cdot \left(\boldsymbol{d}_{i_{n+1}} - \boldsymbol{d}_{i_n}\right) \tag{107}$$

Since the EM scheme satisfies the constraints at the end-point of the time step, see $(104))_3$, result (106) follows. Accordingly, in analogy to the continuous case the discrete constraint forces do no work. Altogether, (105) yields the discrete balance equation for the energy

$$\Delta t \; (\overline{P}_{\text{ext}})\big|_{n+\frac{1}{2}} = \overline{T}_{n+1} - \overline{T}_n$$

Accordingly, if the work of the external loading vanishes, the EM scheme conserves the energy.

Remark 3.2 Instead of using the directionality property (107), result (106) can be obtained as well by a direct calculation. To this end consider the work done by the constraint forces in the time interval $[t_n, t_{n+1}]$:

$$\begin{aligned} \Delta t \; (\boldsymbol{f}^i_{\text{c}})\big|_{n+\frac{1}{2}} \cdot \boldsymbol{v}_{i_{n+\frac{1}{2}}} &= (\boldsymbol{f}^i_{\text{c}})\big|_{n+\frac{1}{2}} \cdot \left(\boldsymbol{d}_{i_{n+1}} - \boldsymbol{d}_{i_n}\right) \\ &= \Lambda^{ij}_{n+1} \boldsymbol{d}_{j_{n+\frac{1}{2}}} \cdot \left(\boldsymbol{d}_{i_{n+1}} - \boldsymbol{d}_{i_n}\right) \\ &= \Lambda^{ij}_{n+1} \tfrac{1}{2}\left(\boldsymbol{d}_{j_{n+1}} + \boldsymbol{d}_{j_n}\right) \cdot \left(\boldsymbol{d}_{i_{n+1}} - \boldsymbol{d}_{i_n}\right) \\ &= \Lambda^{ij}_{n+1} \tfrac{1}{2}\left(d_{ij_{n+1}} - d_{ij_n}\right) \\ &= 0 \end{aligned} \tag{108}$$

Here, it has been taken into account that $(104)_3$ enforces the algebraic constraints at the end-point of each time step such that $d_{ij_n} = d_{ij_{n+1}} = \delta_{ij}$.

Remark 3.3 Whereas the EM scheme (104) enforces the constraints on the position level explicitly through $(104)_3$, this is not the case for the constraints on the velocity level

$$\frac{d}{dt}\hat{g}_l(\boldsymbol{d}_j) = \frac{\partial \hat{g}_l}{\partial \boldsymbol{d}_j} \cdot \boldsymbol{v}_j = 0 \tag{109}$$

However, due to the directionality property (107) of the discrete derivative applied to the constraints, in the discrete setting the relationship

$$\begin{aligned} \overline{\nabla}_{d_i} g_l(\boldsymbol{d}_{j_n}, \boldsymbol{d}_{j_{n+1}}) \cdot \boldsymbol{v}_{i_{n+\frac{1}{2}}} &= \tfrac{1}{\Delta t} \overline{\nabla}_{d_i} g_l(\boldsymbol{d}_{j_n}, \boldsymbol{d}_{j_{n+1}}) \cdot \left(\boldsymbol{d}_{i_{n+1}} - \boldsymbol{d}_{i_n}\right) \\ &= \hat{g}_l(\boldsymbol{d}_{j_{n+1}}) - \hat{g}_l(\boldsymbol{d}_{j_n}) \\ &= 0 \end{aligned}$$

holds. The last equation can be viewed as discrete counterpart of (109). In analogy to (92), the last equation can be recast in the form

$$\boldsymbol{d}_{i_{n+\frac{1}{2}}} \cdot \boldsymbol{v}_{j_{n+\frac{1}{2}}} + \boldsymbol{v}_{i_{n+\frac{1}{2}}} \cdot \boldsymbol{d}_{j_{n+\frac{1}{2}}} = 0$$

Accordingly, the rigid body constraints on the velocity level are satisfied at the mid-point of each time step.

3.6 The Director Triad in the Discrete Setting

The present rigid body formulation is based on the canonical embedding of the rotation group SO(3) into the 9-dimensional linear space. Correspondingly, the 3×3 matrix corresponding to the rotation tensor $\boldsymbol{F} \in \mathrm{SO}(3)$ is viewed as vector in $\mathbb{R}^9$ composed of the three directors $\boldsymbol{d}_i \in \mathbb{R}^3$. Due to the present discretization in time, the configuration constraints are relaxed to specific points in time lying on the boundary of the time intervals $[t_n, t_{n+1}]$ $(n = 0, 1, \ldots)$. Accordingly, for finite time steps $\Delta t = t_{n+1} - t_n$, the orthonormality of the director triad $\{\boldsymbol{d}_i\}$ is generally violated inside the time interval $[t_n, t_{n+1}]$. This observation holds in particular for the mid-points $t_{n+\frac{1}{2}} = \frac{1}{2}(t_n + t_{n+1})$.

3.6.1 Planar Rotations

In a first step we investigate the violation of the orthonormality of the mid-point directors for planar rotations. To this end we consider rotations of the rigid body that take place in the plane spanned by the Cartesian base vectors $\boldsymbol{e}_1$ and $\boldsymbol{e}_2$. By introducing an angle $\alpha \in \mathbb{R}$, the orthonormality of the director frame can be ensured for arbitrarily large rotation angles (see Fig. 7):

$$\widetilde{\boldsymbol{d}}_1(\alpha) = \cos\alpha \boldsymbol{e}_1 + \sin\alpha \boldsymbol{e}_2$$
$$\widetilde{\boldsymbol{d}}_2(\alpha) = -\sin\alpha \boldsymbol{e}_1 + \cos\alpha \boldsymbol{e}_2$$

and $\boldsymbol{d}_3 = \boldsymbol{e}_3$. Since in the discrete setting the orthonormality condition is always enforced at the endpoints of the time steps we write

$$\boldsymbol{d}_{1_n} = \widetilde{\boldsymbol{d}}_1(\alpha_n)\,, \quad \boldsymbol{d}_{1_{n+1}} = \widetilde{\boldsymbol{d}}_1(\alpha_{n+1})$$
$$\boldsymbol{d}_{2_n} = \widetilde{\boldsymbol{d}}_2(\alpha_n)\,, \quad \boldsymbol{d}_{2_{n+1}} = \widetilde{\boldsymbol{d}}_2(\alpha_{n+1})$$

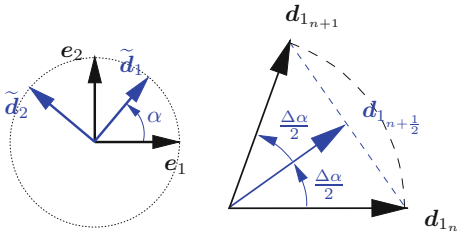

Fig. 7 *Left* Finite rotation of the director frame about the axis $\boldsymbol{e}_3$ with angle α. *Right* Incremental rotation of $\boldsymbol{d}_1$ with angle $\Delta\alpha$ and corresponding mid-point director $\boldsymbol{d}_{1_{n+\frac{1}{2}}}$

where

$$\alpha_{n+1} = \alpha_n + \Delta\alpha$$

so that the incremental rotation from t_n to t_{n+1} is characterized by the angle $\Delta\alpha$. Now a straightforward calculation shows that the mid-point directors $\boldsymbol{d}_{\beta_{n+\frac{1}{2}}}$ ($\beta = 1, 2$) can be written as

$$\begin{aligned} \boldsymbol{d}_{\beta_{n+\frac{1}{2}}} &= \frac{1}{2}\left(\boldsymbol{d}_{\beta_n} + \boldsymbol{d}_{\beta_{n+1}}\right) \\ &= A(\Delta\alpha)\widetilde{\boldsymbol{d}}_\beta(\alpha_{n+\frac{1}{2}}) \end{aligned}$$

where $\alpha_{n+\frac{1}{2}} = \frac{1}{2}(\alpha_n + \alpha_{n+1})$, and

$$A(\Delta\alpha) = \cos\left(\frac{\Delta\alpha}{2}\right)$$

Accordingly, the mid-point approximation of the directors is still orthogonal, for

$$\boldsymbol{d}_{1_{n+\frac{1}{2}}} \cdot \boldsymbol{d}_{2_{n+\frac{1}{2}}} = \left(A(\Delta\alpha)\right)^2 \widetilde{\boldsymbol{d}}_1(\alpha_{n+\frac{1}{2}}) \cdot \widetilde{\boldsymbol{d}}_2(\alpha_{n+\frac{1}{2}}) = 0$$

but generally fails to be of unit length (see also Fig. 7). In particular, we have

$$\begin{aligned} \boldsymbol{d}_{(\beta)_{n+\frac{1}{2}}} \cdot \boldsymbol{d}_{(\beta)_{n+\frac{1}{2}}} &= \left(A(\Delta\alpha)\right)^2 \parallel \widetilde{\boldsymbol{d}}_\beta(\alpha_{n+\frac{1}{2}}) \parallel^2 \\ &= \tfrac{1}{2}\left(1 + \cos(\Delta\alpha)\right) \\ &\leq 1 \end{aligned} \tag{110}$$

To summarize, in the case of planar rotations, the mid-point directors stay mutually orthogonal but their length is reduced. Note that this discretization error decreases if the rotation increment (or time step) is reduced.

3.6.2 Three-dimensional Rotations

In the three-dimensional setting the mid-point directors are in general neither of unit length, nor mutually orthogonal. That is, $\boldsymbol{d}_{i_{n+\frac{1}{2}}} \cdot \boldsymbol{d}_{j_{n+\frac{1}{2}}} \neq \delta_{ij}$ in general. In particular, a lengthy but straightforward calculation, employing the well-known formula (Bottema and Roth 1979; Hughes and Winget 1980)

$$\boldsymbol{d}_{i_{n+1}} - \boldsymbol{d}_{i_n} = \boldsymbol{\vartheta} \times \boldsymbol{d}_{i_{n+\frac{1}{2}}}$$

shows that

$$\boldsymbol{d}_{i_{n+\frac{1}{2}}} \cdot \boldsymbol{B}(\boldsymbol{\vartheta})\boldsymbol{d}_{j_{n+\frac{1}{2}}} = \delta_{ij} \tag{111}$$

where

$$\boldsymbol{B}(\boldsymbol{\vartheta}) = \left(1 + \frac{1}{4}\boldsymbol{\vartheta}\cdot\boldsymbol{\vartheta}\right)\boldsymbol{I} - \frac{1}{4}\boldsymbol{\vartheta}\otimes\boldsymbol{\vartheta}$$

Thus, in the limit case of vanishing incremental rotations (i.e., $\boldsymbol{\vartheta} = \boldsymbol{0}$) we get $\boldsymbol{B}(\boldsymbol{0}) = \boldsymbol{I}$, and the orthonormality of the mid-point directors is recovered.

Moreover, if $\boldsymbol{\vartheta}\cdot\boldsymbol{d}_{i_{n+\frac{1}{2}}} = 0$, such as in the planar case, Eq. (111) yields

$$\left(1 + \frac{1}{4}\boldsymbol{\vartheta}\cdot\boldsymbol{\vartheta}\right)\boldsymbol{d}_{i_{n+\frac{1}{2}}}\cdot\boldsymbol{d}_{j_{n+\frac{1}{2}}} = \delta_{ij}$$

Accordingly, the mid-point directors are mutually orthogonal. In addition to that, the relation $\boldsymbol{d}_{(i)_{n+\frac{1}{2}}}\cdot\boldsymbol{d}_{(i)_{n+\frac{1}{2}}} = (1 + \frac{1}{4}\boldsymbol{\vartheta}\cdot\boldsymbol{\vartheta})^{-1}$ shows that the length of the mid-point directors is generally smaller than one. This result is in agreement with (110). In particular, it can be shown that

$$\begin{aligned}(A(\Delta\alpha))^2 &= \tfrac{1}{2}\left(1 + \cos(\Delta\alpha)\right)\\ &= \left(1 + \left(\tfrac{\|\boldsymbol{\vartheta}\|}{2}\right)^2\right)^{-1}\end{aligned}$$

for $\frac{\|\boldsymbol{\vartheta}\|}{2} = \tan(\frac{\Delta\alpha}{2})$.

Remark 3.4 Similar geometric considerations apply to the elastic Cosserat point. In particular, the application of the mid-point rule rests on the Green–Lagrangean strains

$$\gamma_{ij}^{\mathrm{MP}} = \frac{1}{2}\left(d_{ij}^{\mathrm{MP}} - \delta_{ij}\right) \tag{112}$$

where

$$d_{ij}^{\mathrm{MP}} = \boldsymbol{d}_{i_{n+\frac{1}{2}}}\cdot\boldsymbol{d}_{j_{n+\frac{1}{2}}}$$

Accordingly, if the elastic Cosserat point undergoes finite rotations, the mid-point rule in general generates artificial strains. This discretization error is especially pronounced for stiff material behavior and might trigger spurious oscillations leading to numerical instabilities. Originally, artificial normal strains produced by the mid-point rule have been observed in the context of an elastic pendulum (Tarnow 1993; Crisfield and Shi 1994).

3.7 The Link to Natural Coordinates

The present formulation of rigid body dynamics is closely related to the notion of natural coordinates advocated by García de Jalón and co-workers (García de Jalón

2007). This can be easily shown by considering the connection between the present coordinates and the natural coordinates associated with the *most general element* (García de Jalón and Bayo 1994). The configuration of the most general element is specified by

$$\boldsymbol{q}^e = \left[\boldsymbol{r}_A^T \ \boldsymbol{r}_B^T \ \boldsymbol{u}^T \ \boldsymbol{v}^T\right]^T \tag{113}$$

where $\boldsymbol{r}_A, \boldsymbol{r}_B \in \mathbb{R}^3$ denote the position vectors of two basic points A, B, and $\boldsymbol{u}, \boldsymbol{v} \in \mathbb{R}^3$ denote two non-coplanar unit vectors (Fig. 8). The natural coordinates in (113) can now be expressed in terms of the present coordinates:

$$\begin{aligned} \boldsymbol{r}_A &= \bar{\boldsymbol{x}} + X_A^i \boldsymbol{d}_i \\ \boldsymbol{r}_B &= \bar{\boldsymbol{x}} + X_B^i \boldsymbol{d}_i \end{aligned} \quad \text{and} \quad \begin{aligned} \boldsymbol{u} &= U^i \boldsymbol{d}_i \\ \boldsymbol{v} &= V^i \boldsymbol{d}_i \end{aligned}$$

Here X_A^i, X_B^i are the material coordinates of points A, B, and U^i, V^i are the components of the unit vectors $\boldsymbol{u}$, $\boldsymbol{v}$ relative to the director (or body) frame. Alternatively, we may write

$$\boldsymbol{q}^e = \boldsymbol{T}\boldsymbol{q}$$

where $\boldsymbol{q} \in \mathbb{R}^{12}$ contains the present coordinates according to (58), and $\boldsymbol{T}$ is a 12×12 transformation matrix of the form

$$\boldsymbol{T} = \begin{bmatrix} \boldsymbol{I} & X_A^1 \boldsymbol{I} & X_A^2 \boldsymbol{I} & X_A^3 \boldsymbol{I} \\ \boldsymbol{I} & X_B^1 \boldsymbol{I} & X_B^2 \boldsymbol{I} & X_B^3 \boldsymbol{I} \\ \boldsymbol{0} & U^1 \boldsymbol{I} & U^2 \boldsymbol{I} & U^3 \boldsymbol{I} \\ \boldsymbol{0} & V^1 \boldsymbol{I} & V^2 \boldsymbol{I} & V^3 \boldsymbol{I} \end{bmatrix}$$

The mass matrix pertaining to the most general element is given by

$$\boldsymbol{M}^e = \boldsymbol{T}^T \boldsymbol{M} \boldsymbol{T}$$

where the constant mass matrix $\boldsymbol{M}$ of the present formulation is given by (60). Since $\boldsymbol{T}$ is *constant*, $\boldsymbol{M}^e$ is constant too. The connection between further rigid body elements

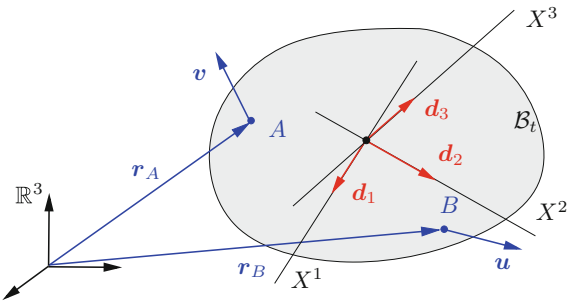

Fig. 8 Connection between the present director formulation and natural coordinates

belonging to the family of elements provided by the natural coordinates approach can be found in García de Jalón and Bayo (1994, Sect. 4.2.2).

3.8 Application of External Torques

The application of external torques $\overline{\boldsymbol{m}}_{\text{ext}}$ relative to the center of mass of the rigid body can be accomplished via the external director forces $\boldsymbol{f}^i_{\text{ext}}$, cf. (71). For this purpose one may use

$$\begin{bmatrix} \boldsymbol{f}^1_{\text{ext}} \\ \boldsymbol{f}^2_{\text{ext}} \\ \boldsymbol{f}^3_{\text{ext}} \end{bmatrix} = \frac{1}{2\sqrt{d}} \begin{bmatrix} \boldsymbol{d}_2 \otimes \boldsymbol{d}_3 - \boldsymbol{d}_3 \otimes \boldsymbol{d}_2 \\ \boldsymbol{d}_3 \otimes \boldsymbol{d}_1 - \boldsymbol{d}_1 \otimes \boldsymbol{d}_3 \\ \boldsymbol{d}_1 \otimes \boldsymbol{d}_2 - \boldsymbol{d}_2 \otimes \boldsymbol{d}_1 \end{bmatrix} \overline{\boldsymbol{m}}_{\text{ext}} = \frac{1}{2} \begin{bmatrix} \overline{\boldsymbol{m}}_{\text{ext}} \times \boldsymbol{d}^1 \\ \overline{\boldsymbol{m}}_{\text{ext}} \times \boldsymbol{d}^2 \\ \overline{\boldsymbol{m}}_{\text{ext}} \times \boldsymbol{d}^3 \end{bmatrix}$$

This relationship is derived in Appendix A.2. In the discrete setting we make use of

$$(\boldsymbol{f}^i_{\text{ext}})\big|_{n+\frac{1}{2}} = \frac{1}{2}\, \overline{\boldsymbol{m}}_{\text{ext}}|_{n+\frac{1}{2}} \times \boldsymbol{d}^i\big|_{n+\frac{1}{2}} \tag{114}$$

Here, $\overline{\boldsymbol{m}}_{\text{ext}}|_{n+\frac{1}{2}}$ represents an external torque applied in the time interval $[t_n, t_{n+1}]$, and $\boldsymbol{d}^i\big|_{n+\frac{1}{2}}$ are contravariant mid-point directors that satisfy the condition

$$\boldsymbol{d}^i\big|_{n+\frac{1}{2}} \cdot \boldsymbol{d}_{j_{n+\frac{1}{2}}} = \delta^i_j$$

To satisfy the balance of angular momentum in the discrete setting, it is of paramount importance to distinguish between covariant mid-point directors, $\boldsymbol{d}_{j_{n+\frac{1}{2}}}$, and associated contravariant (or dual) mid-point directors, $\boldsymbol{d}^i\big|_{n+\frac{1}{2}}$. This fact is closely related to the properties of the mid-point directors investigated in Sect. 3.6. Formula (114) has originally been proposed in Betsch et al. (2012), see also Betsch and Sänger (2013) and Koch and Leyendecker (2013).

3.9 Balance of Angular Momentum in the Discrete Setting

We next prove that formula (114) does indeed make possible the consistent application of external torques. To this end we consider the discrete counterpart of the continuous relationship $\frac{d}{dt}\bar{\boldsymbol{j}} = \overline{\boldsymbol{m}}_{\text{ext}}$, see $(96)_2$, which is given by

$$\bar{\boldsymbol{j}}_{n+1} - \bar{\boldsymbol{j}}_n = \Delta t \boldsymbol{d}_{j_{n+\frac{1}{2}}} \times (\boldsymbol{f}^j_{\text{ext}})\Big|_{n+\frac{1}{2}}$$

cf. (70). Inserting from (114) yields

$$\begin{aligned}\bar{\boldsymbol{j}}_{n+1} - \bar{\boldsymbol{j}}_n &= \frac{\Delta t}{2} \boldsymbol{d}_{i_{n+\frac{1}{2}}} \times \left(\overline{\boldsymbol{m}}_{\text{ext}}|_{n+\frac{1}{2}} \times \boldsymbol{d}^i\big|_{n+\frac{1}{2}} \right) \\ &= \frac{\Delta t}{2} \left((\boldsymbol{d}_{i_{n+\frac{1}{2}}} \cdot \boldsymbol{d}^i\big|_{n+\frac{1}{2}})\, \overline{\boldsymbol{m}}_{\text{ext}}|_{n+\frac{1}{2}} - (\boldsymbol{d}_{i_{n+\frac{1}{2}}} \cdot \overline{\boldsymbol{m}}_{\text{ext}}|_{n+\frac{1}{2}})\, \boldsymbol{d}^i\big|_{n+\frac{1}{2}} \right) \\ &= \Delta t\, \overline{\boldsymbol{m}}_{\text{ext}}|_{n+\frac{1}{2}}\end{aligned} \tag{115}$$

Consequently, formula (114) guarantees that external torques are properly applied in the discrete setting.

4 Extension to Multibody Dynamics

So far we focused on a single Cosserat point and a single rigid body. However, the present framework can be easily extended to nonlinear structural dynamics and flexible multibody dynamics by applying Cosserat theories for the description of nonlinear beams and shells (Rubin 2000; Antman 2005; Bauchau 2011). Further details of the extension of the present approach to more complicated mechanical systems may be found in Betsch and Steinmann (2002b, c, 2003), Betsch (2006), Betsch and Leyendecker (2006), Leyendecker et al. (2006, 2008a), Betsch and Uhlar (2007), Betsch and Sänger (2009a, b).

In this work we illustrate the extension of the present approach to classical multibody systems, comprised of rigid bodies. First we consider the formulation of kinematic pairs.

4.1 Kinematic Pairs

We next illustrate the formulation of kinematic pairs with the example of a cylindrical pair (Fig. 9). To this end we consider two rigid bodies formulated as constrained mechanical systems as described in Sect. 3. Accordingly, the configuration of the two-body system under consideration is characterized by redundant coordinates

$$\boldsymbol{q} = \begin{bmatrix} {}^1\boldsymbol{q} \\ {}^2\boldsymbol{q} \end{bmatrix} \quad \text{where} \quad {}^\alpha\boldsymbol{q} = \begin{bmatrix} {}^\alpha\boldsymbol{\varphi} \\ {}^\alpha\boldsymbol{d}_1 \\ {}^\alpha\boldsymbol{d}_2 \\ {}^\alpha\boldsymbol{d}_3 \end{bmatrix} \tag{116}$$

Note that the contribution of body α to the configuration vector coincides with (58). The equations of motion pertaining to the constrained mechanical system at hand can again be formulated as outlined in Sect. 3. Similar to (116), the contribution of

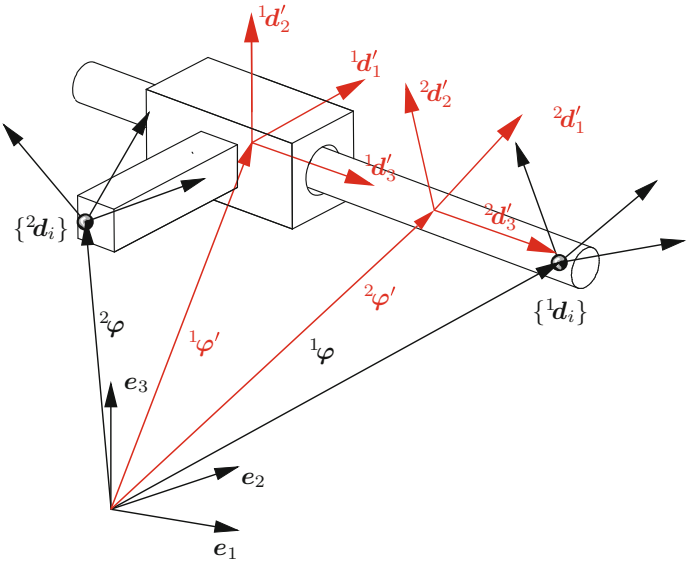

Fig. 9 Sketch of the cylindrical pair: Coordinates $({}^\alpha\boldsymbol{\varphi}, \{{}^\alpha\boldsymbol{d}_i\})$ characterizing the current configuration ${}^\alpha\mathcal{B}_t$ of rigid body α. The additional systems $({}^\alpha\boldsymbol{\varphi}', \{{}^\alpha\boldsymbol{d}'_i\})$ are introduced for the description of the motion of the second body relative to the first body (translation along and rotation about ${}^1\boldsymbol{d}'_3 = {}^2\boldsymbol{d}'_3$). The connection between $({}^\alpha\boldsymbol{\varphi}', \{{}^\alpha\boldsymbol{d}'_i\})$ and the coordinates $({}^\alpha\boldsymbol{\varphi}, \{{}^\alpha\boldsymbol{d}_i\})$ is defined in the initial configuration of the multibody system

each rigid body to the external forces leads to the system vector

$$\boldsymbol{F} = \begin{bmatrix} {}^1\boldsymbol{F} \\ {}^2\boldsymbol{F} \end{bmatrix} \quad \text{where} \quad {}^\alpha\boldsymbol{F} = \begin{bmatrix} {}^\alpha\boldsymbol{f}_\varphi \\ {}^\alpha\boldsymbol{f}^1 \\ {}^\alpha\boldsymbol{f}^2 \\ {}^\alpha\boldsymbol{f}^3 \end{bmatrix} \tag{117}$$

Note that the force vector ${}^\alpha\boldsymbol{F}$ associated with body α coincides with (61).

4.1.1 Initialization of Kinematic Relationships

To describe the motion of the second body relative to the first one we introduce orthonormal body-fixed triads $\{{}^\alpha\boldsymbol{d}'_i\}$ in such a way that the unit vectors ${}^\alpha\boldsymbol{d}'_3$ are parallel to the axis of the cylindrical pair (Fig. 9). Moreover, we choose the two orthonormal triads to coincide in the initial configuration, i.e. ${}^1\boldsymbol{d}'_i(0) = {}^2\boldsymbol{d}'_i(0)$. The connection between the newly introduced orthonormal triads $\{{}^\alpha\boldsymbol{d}'_i\}$ and the original triads $\{{}^\alpha\boldsymbol{d}_i\}$ is given by

$${}^\alpha\boldsymbol{R}' = {}^\alpha\boldsymbol{F}\,{}^\alpha\boldsymbol{\Lambda}_0 \tag{118}$$

where

$$ {}^{\alpha}\boldsymbol{F} = {}^{\alpha}\boldsymbol{d}_i \otimes \boldsymbol{e}^i \quad \text{and} \quad {}^{\alpha}\boldsymbol{R}' = {}^{\alpha}\boldsymbol{d}_i' \otimes \boldsymbol{e}^i $$

The constant tensors ${}^{\alpha}\boldsymbol{\Lambda}_0$ in (118) are calculated in the initial configuration via

$$ {}^{\alpha}\boldsymbol{\Lambda}_0 = {}^{\alpha}\boldsymbol{F}^{-1}(0)\, {}^{\alpha}\boldsymbol{R}'(0) $$

The origin of the newly introduced orthonormal triads $\{{}^{\alpha}\boldsymbol{d}_i'\}$ is fixed at material points ${}^{\alpha}\Theta^i$ whose placement in the current configuration ${}^{\alpha}\mathcal{B}_t$ of rigid body α is denoted by ${}^{\alpha}\boldsymbol{\varphi}'$. Accordingly,

$$ {}^{\alpha}\boldsymbol{\varphi}' = {}^{\alpha}\boldsymbol{\varphi} + {}^{\alpha}\Theta^i\, {}^{\alpha}\boldsymbol{d}_i $$

Note that the location of the material points ${}^{\alpha}\Theta^i$ has to be specified during initialization.

4.1.2 Configuration Space of the Cylindrical Pair

The configuration space of the cylindrical pair can be easily defined by distinguishing between internal constraints due the assumption of rigidity and external constraints due to the interconnection between the rigid bodies in a multibody system (Betsch and Steinmann 2002c). Accordingly, the present description of the cylindrical pair relies on $n = 24$ coordinates subject to 12 internal constraints $\boldsymbol{g}^{\text{int}}({}^{\alpha}\boldsymbol{q}) = \boldsymbol{0}\,(\alpha = 1, 2)$, where $\boldsymbol{g}^{\text{int}} : \mathbb{R}^{12} \to \mathbb{R}^6$ follows from (89), and 4 external constraints associated with the constraint functions

$$ \boldsymbol{g}_{\text{P}}^{\text{ext}}(\boldsymbol{q}) = \begin{bmatrix} {}^{1}\boldsymbol{d}_1' \cdot \left({}^{2}\boldsymbol{\varphi}' - {}^{1}\boldsymbol{\varphi}'\right) \\ {}^{1}\boldsymbol{d}_2' \cdot \left({}^{2}\boldsymbol{\varphi}' - {}^{1}\boldsymbol{\varphi}'\right) \end{bmatrix} \tag{119} $$

and

$$ \boldsymbol{g}_{\text{R}}^{\text{ext}}(\boldsymbol{q}) = \begin{bmatrix} {}^{1}\boldsymbol{d}_1' \cdot {}^{2}\boldsymbol{d}_3' \\ {}^{1}\boldsymbol{d}_2' \cdot {}^{2}\boldsymbol{d}_3' \end{bmatrix} \tag{120} $$

To summarize, we have $n = 24$ coordinates subject to $m = 16$ constraints which can be assembled in the constraint function $\boldsymbol{g}^{\text{C}} : \mathbb{R}^{24} \to \mathbb{R}^{16}$ given by

$$ \boldsymbol{g}^{\text{C}}(\boldsymbol{q}) = \begin{bmatrix} \boldsymbol{g}^{\text{int}}({}^{1}\boldsymbol{q}) \\ \boldsymbol{g}^{\text{int}}({}^{2}\boldsymbol{q}) \\ \boldsymbol{g}_{\text{P}}^{\text{ext}}(\boldsymbol{q}) \\ \boldsymbol{g}_{\text{R}}^{\text{ext}}(\boldsymbol{q}) \end{bmatrix} \tag{121} $$

Consequently, the configuration space of the cylindrical pair is defined by

$$ \mathsf{Q}^{\text{C}} = \{\boldsymbol{q} \in \mathbb{R}^{24} \,|\, \boldsymbol{g}^{\text{C}}(\boldsymbol{q}) = \boldsymbol{0}\} \tag{122} $$

4.2 Multibody Systems

As mentioned before, geometrically exact Cosserat models for beams and shells fit perfectly well into the present framework. In particular, if the nonlinear beam and shell formulations are discretized in space as proposed in Betsch and Steinmann (2002b, 2003), Betsch and Sänger (2009a), the equations of motion pertaining to the resulting discrete mechanical systems fit into the framework outlined in Sect. 3. Thus the use of director coordinates makes possible a uniform formulation of flexible multibody dynamics.[2] Main characteristics of the present approach can be summarized as follows:

1. The inertia parameters are always constant leading to the simple structure of the inertia terms in the equations of motion. In particular, the differential part of the equations of motion can be written as

$$\boldsymbol{M}\ddot{\boldsymbol{q}} + \nabla V_\lambda(\boldsymbol{q}) - \boldsymbol{F} = \boldsymbol{0}$$

   where the potential forces along with the constraint forces can be derived from an augmented potential function of the form

$$V_\lambda(\boldsymbol{q}) = U(\boldsymbol{q}) + \sum_{l=1}^{m} \lambda^l \nabla g_l(\boldsymbol{q})$$

   For example, the potential function $U(\boldsymbol{q})$ can be associated with the action of gravitational forces or with the deformation of flexible bodies such as nonlinear beams and shells relying on hyperelastic constitutive laws.
2. The configuration vector of the complete flexible multibody systems is composed of vectors $\boldsymbol{q}_I \in \mathbb{R}^3$ and thus given by

$$\boldsymbol{q} = \begin{bmatrix} \boldsymbol{q}_1 \\ \boldsymbol{q}_2 \\ \vdots \\ \boldsymbol{q}_N \end{bmatrix} \tag{123}$$

   where N denotes the total number of 3-vectors $\boldsymbol{q}_I$ needed to describe a specific multibody system. Accordingly, in total, the configuration vector $\boldsymbol{q} \in \mathbb{R}^n$ has $n = 3N$ components.
3. The total angular momentum of flexible multibody systems can be cast in the form

$$\boldsymbol{J} = \sum_{a,b=1}^{N} M^{ab} \boldsymbol{q}_a \times \boldsymbol{v}_b \tag{124}$$

[2] The present framework comprises as well domain decomposition problems (Hesch and Betsch 2010) and large deformation contact (Hesch and Betsch 2009, 2011a, b).

where M^{ab} contain the constant inertia parameters and $\boldsymbol{v}_b = \dot{\boldsymbol{q}}_b$.

4. The balance of angular momentum can be written as

$$\frac{d}{dt}\boldsymbol{J} = \sum_{a=1}^{N} \boldsymbol{q}_a \times \left(\boldsymbol{F}^a - \nabla_{\boldsymbol{q}_a} V_\lambda(\boldsymbol{q})\right) \tag{125}$$

The EM consistent discretization of the discrete mechanical systems at hand can be performed in complete analogy to the Cosserat point and the rigid body dealt with in detail in the previous sections.

5 Numerical Examples

5.1 Spacecraft Attitude Maneuver

In the first numerical example we demonstrate the importance of formula (114) for the consistent application of external torques. To this end we apply the present approach to the control of spacecraft rotational maneuvers.

The spacecraft is modeled as multibody system consisting of four rigid bodies (Fig. 10), namely the base body and three reaction wheels. A similar example has been dealt with in Leyendecker et al. (2010). The data for the present 4-body system

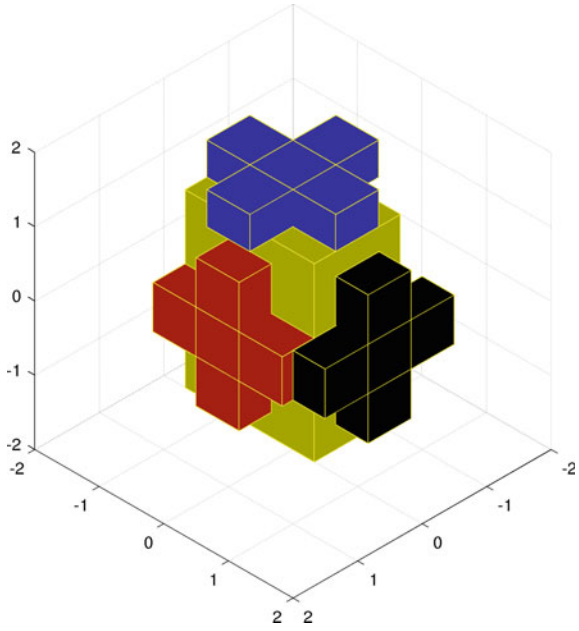

Fig. 10 The spacecraft as 4-body system

Table 1 Spacecraft: data for the 4-body system

Body	M_φ	E^{11}	E^{22}	E^{33}	L
1	1005.3096	89.3609	201.0619	357.4434	
2	424.1150	8.8357	106.0288	106.0288	0.9167
3	424.1150	106.0288	8.8357	106.0288	1.25
4	424.1150	106.0288	106.0288	8.8357	1.5833

Note that L denotes the distance between the center of mass of the reaction wheels and the base body

have been taken from (Leyendecker et al. 2010). Using principal axis for each rigid body the data used in the simulations are summarized in Table 1.

The reaction wheels are spinning about body-fixed axis of the base body. For simplicity the three body-fixed axis are assumed to coincide with the director frame $\{{}^1\boldsymbol{d}_i\}$ of the base body. Spacecraft attitude maneuvers are performed by applying reaction wheel motor torques

$$ {}^2\boldsymbol{m} = (u^1)\,{}^1\boldsymbol{d}_1\,, \quad {}^3\boldsymbol{m} = (u^2)\,{}^1\boldsymbol{d}_2\,, \quad {}^4\boldsymbol{m} = (u^3)\,{}^1\boldsymbol{d}_3 \tag{126} $$

In the example we prescribe constant motor torques $u^i = 200$.

A total of $n = 48$ coordinates are employed to describe the multibody system at hand. Each body is subject to 6 rigid body constraints giving rise to $m^{\text{int}} = 24$ internal constraints. Revolute joints are used to connect the reaction wheels to the base body. This amounts to $m^{\text{ext}} = 3 \times 5 = 15$ external constraints. Accordingly, in total there are $m = m^{\text{int}} + m^{\text{ext}} = 39$ independent constraints leading to $n - m = 9$ degrees of freedom.

The newly devised formula (114) has been used to consistently apply the motor torques to the reaction wheels. The torque acting on the base body is given by

$$ {}^1\boldsymbol{m} = -\left({}^2\boldsymbol{m} + {}^3\boldsymbol{m} + {}^4\boldsymbol{m}\right) \tag{127} $$

Since no resultant external torque acts on the spacecraft, the total angular momentum is a first integral of the motion. In particular,

$$ \begin{aligned} \boldsymbol{J}_{n+1} - \boldsymbol{J}_n &= \Delta t \sum_{b=1}^{4} {}^b\boldsymbol{d}_{i_{n+\frac{1}{2}}} \times {}^b\boldsymbol{f}^i\big|_{n+\frac{1}{2}} \\ &= \frac{\Delta t}{2} \sum_{b=1}^{4} {}^b\boldsymbol{d}_{i_{n+\frac{1}{2}}} \times \left({}^b\boldsymbol{m} \times {}^b\boldsymbol{d}^i\big|_{n+\frac{1}{2}}\right) \\ &= \frac{\Delta t}{2} \sum_{b=1}^{4} \left(({}^b\boldsymbol{d}_{i_{n+\frac{1}{2}}} \cdot {}^b\boldsymbol{d}^i)\,{}^b\boldsymbol{m} - ({}^b\boldsymbol{d}_{i_{n+\frac{1}{2}}} \cdot {}^b\boldsymbol{m})\,{}^b\boldsymbol{d}^i\big|_{n+\frac{1}{2}}\right) \\ &= \Delta t \sum_{b=1}^{4} {}^b\boldsymbol{m} \\ &= \boldsymbol{0} \end{aligned} $$

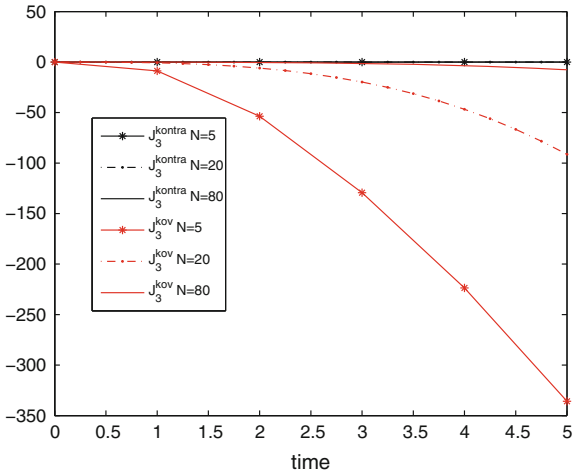

Fig. 11 Spacecraft: Comparison of angular momentum

where use has been made of (126) and (127). In the numerical simulations we focus on the 3-component J_3 of the total angular momentum and the total kinetic energy T of the multibody system at hand. The numerical results due to the application of the newly devised formula (114) are denoted by J_3^{kontra} and T^{kontra}.

For comparison we apply the motor torques via the straightforward mid-point evaluation of the continuous expression of the 'original' formulation (Betsch et al. 2012).

$$\boldsymbol{f}_{i_{n+\frac{1}{2}}} = \frac{1}{2}\boldsymbol{m}_{n+\frac{1}{2}} \times \boldsymbol{d}_{i_{n+\frac{1}{2}}} \tag{128}$$

The corresponding results are denoted by J_3^{kov} and T^{kov}.

A number of N time steps is used to resolve the time interval $[0, 5]$. It can be observed from Fig. 11 that J_3^{kontra} stays constant for all N. This corroborates algorithmic conservation of the total angular momentum. In severe contrast to that J_3^{kov} does not stay constant. Accordingly the balance law for angular momentum is violated. This discretization error can be decreased by raising the number of time steps N. These observations are further supported by considering the total kinetic energy in Fig. 12. Accordingly, T^{kontra} does hardly change if the time steps are refined. That is, using only $N = 5$ time steps already leads to a very good approximation of the kinetic energy. This is in severe contrast to T^{kov}.

5.2 *Parallel Robot*

In the second example we consider the planar parallel robot depicted in Fig. 13. Each of the three legs of the parallel robot consists of a prismatic kinematic pair along with two revolute joints. The parallel mechanism has three degrees of freedom and

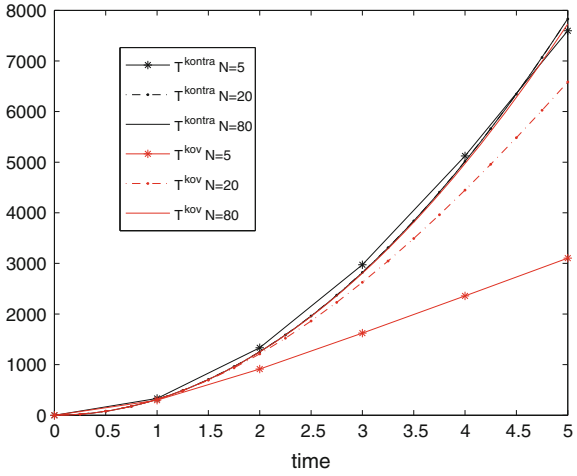

Fig. 12 Spacecraft: Comparison of kinetic energy

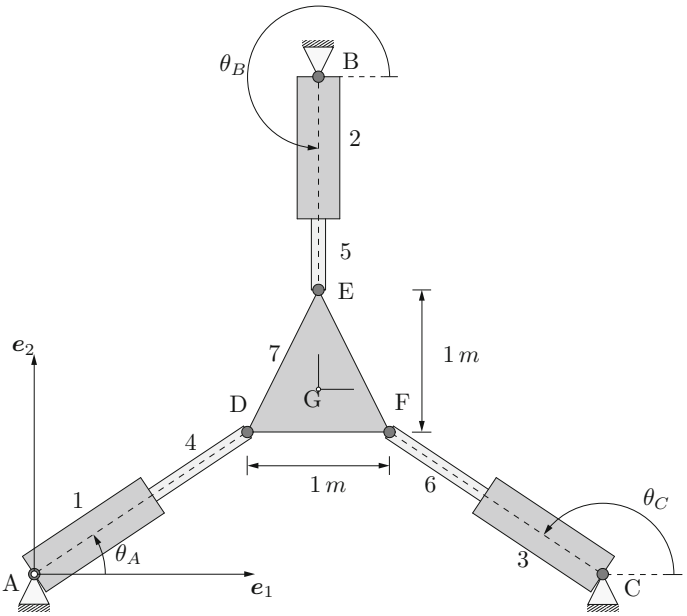

Fig. 13 The 3-RPR planar parallel robot

is referred to as the 3-RPR planar parallel manipulator, where the underlined letter indicates that one of the revolute joints of each leg is driven.

In the forward dynamics simulation we rely on the results of an inverse dynamics analysis due to McPhee and Redmond (2006). The goal of the inverse dynamics

analysis is to determine the driving torques required to translate the center of mass G of the end-effector in a figure-8 pattern, with a cycle time of 2 s, defined by

$$\begin{aligned} x_G &= 2 + \sin(\pi t) \\ y_G &= \frac{4}{3} + \frac{1}{2}\sin(2\pi t) \\ \theta_G &= 0 \end{aligned} \tag{129}$$

The geometry and inertia properties of the parallel robot have been taken as well from McPhee and Redmond (2006) and are summarized in Table 2. In addition to that, we remark that the position of points B and C (Fig. 13) is given by $x_B = 2$, $y_B = 3.5$, and $x_C = 4.0$. The result of the inverse dynamics analysis gives rise to the three driving torques, one of which is depicted in Fig. 14 (compare with Fig. 12 in McPhee and Redmond 2006).

Obviously, using the three driving torques from the inverse dynamics analysis in the forward dynamics simulation along with the data in Table 2 should lead to the motion of the end-effector given by (129). That is, the trajectory of the center of mass G of the end-effector should follow a figure-8 pattern, while the end-effector should not rotate.

In the simulation we use 200 time steps and apply formula (114) for the consistent application of external torques. It can be observed from Fig. 15 that the proposed

Table 2 Geometry and inertia properties of the parallel robot

Body	Width (m)	Length (m)	Mass (kg)	Moment of inertia (kg m^2)
1, 2, 3	0.3	1.0	2.4	0.218
4, 5, 6	0.1	1.5	1.2	0.226
7	1.0	1.0	0.5	0.049

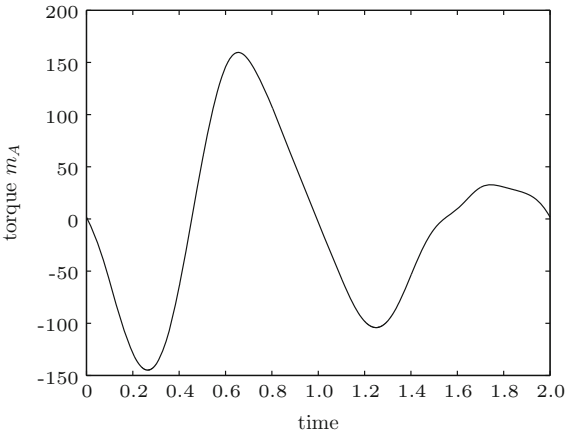

Fig. 14 Parallel robot: Driving torque at joint A determined by the inverse dynamics analysis

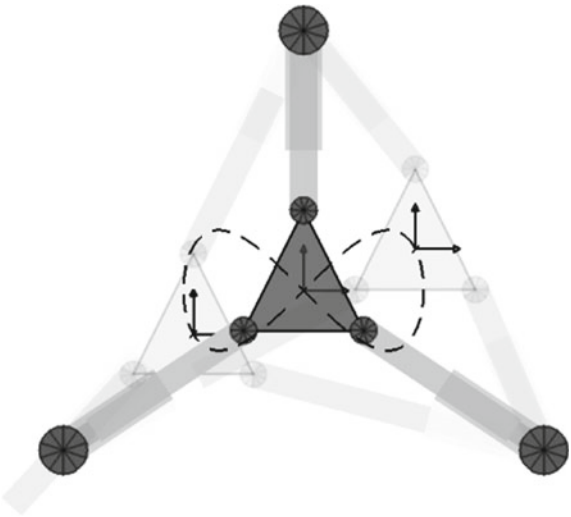

Fig. 15 Parallel robot: Final position simulated with the proposed method. The figure-8 trajectory is correctly tracked by the mass center of the end-effector

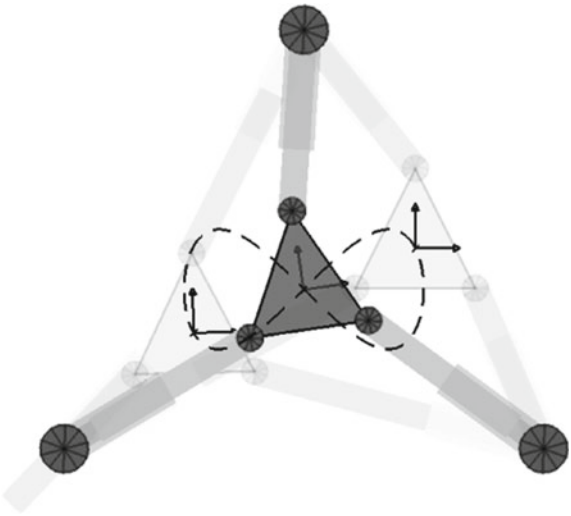

Fig. 16 Parallel robot: Final position simulated with the original method. The inconsistent application of the driving torques leads to a deviation from the correct motion

simulation method yields the correct motion. In sharp contrast to that, using instead of formula (114) the mid-point evaluation of the original formulation, Eq. (128), yields a deviation from the correct motion (Fig. 16). This observation is further supported by Fig. 17, where the rotation angle of the end-effector is plotted versus time. While the advocated method correctly reproduces the constant angle $\theta_G^{kontra} = 0$, the angle θ_G^{kov} determined by the original approach deviates significantly from the correct value. These results strongly support the need for a consistent formulation of external torques in the underlying rotationless formulation.

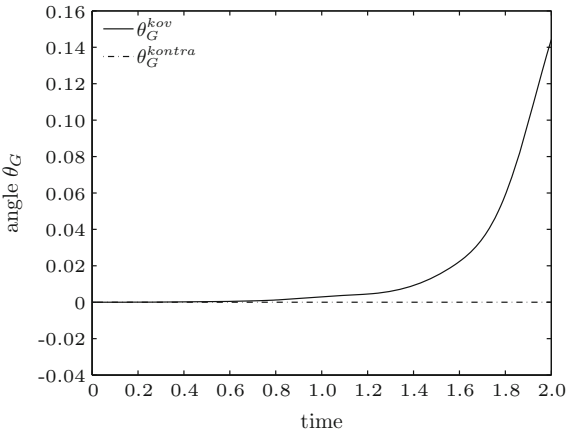

Fig. 17 Parallel robot: Rotation angle of the end-effector

Acknowledgments Support for this research was provided by the Deutsche Forschungsgemeinschaft (DFG) under Grant BE 2285/10-1. This support is gratefully acknowledged.

A Appendix

A.1 Balance Laws

For comparison, the balance laws are directly derived from the variational equations (19) governing the motion of the pseudo-rigid body. To this end, we recast (19) in the form

$$\delta\overline{\boldsymbol{x}} \cdot \left(M\ddot{\overline{\boldsymbol{x}}} - \boldsymbol{f}_{\text{ext}}\right) = 0 \tag{130}$$

$$\operatorname{tr}\left(\delta\boldsymbol{F}^T\left(\ddot{\boldsymbol{F}}\boldsymbol{E}_0 + 2\boldsymbol{F}DU(\boldsymbol{C}) - \boldsymbol{M}_{\text{ext}}\right)\right) = 0 \tag{131}$$

Applying the polar decomposition theorem to the deformation gradient, we get

$$\boldsymbol{F} = \boldsymbol{R}\boldsymbol{U} \qquad \text{and} \qquad \delta\boldsymbol{F} = \delta\boldsymbol{R}\boldsymbol{U} + \boldsymbol{R}\delta\boldsymbol{U} \tag{132}$$

Since $\boldsymbol{R}\boldsymbol{R}^T = \boldsymbol{I}$, $\delta\boldsymbol{R}\boldsymbol{R}^T + \boldsymbol{R}\delta\boldsymbol{R}^T = \boldsymbol{0}$, and consequently

$$\widehat{\boldsymbol{\omega}}_\delta = \delta\boldsymbol{R}\boldsymbol{R}^T \tag{133}$$

is skew-symmetric. A straightforward calculation shows that (131) can be rewritten as

$$\operatorname{tr}\left(\delta\boldsymbol{U}\boldsymbol{U}\left(\boldsymbol{F}^{-1}\ddot{\boldsymbol{F}}\boldsymbol{E}_0 + 2DU(\boldsymbol{C}) - \boldsymbol{F}^{-1}\boldsymbol{M}_{\text{ext}}\right)\right) = 0 \tag{134}$$

$$\boldsymbol{\omega}_\delta \cdot \left(2\text{vect}\left(\ddot{\boldsymbol{F}}\boldsymbol{E}_0\boldsymbol{F}^T\right) - 2\text{vect}\left(\boldsymbol{M}_{\text{ext}}\boldsymbol{F}^T\right)\right) = 0 \tag{135}$$

Accordingly, the nine independent equations emanating from (131) have been converted to six independent equations (134) plus three independent equations (135). In (135), vect(•) denotes the vector invariant of a second-order tensor defined by

$$\text{vect}(\boldsymbol{a}\otimes\boldsymbol{b})\times\boldsymbol{c}=\text{skew}(\boldsymbol{a}\otimes\boldsymbol{b})\boldsymbol{c}$$

Since

$$\begin{aligned}\text{skew}(\boldsymbol{a}\otimes\boldsymbol{b})\boldsymbol{c}&=\frac{1}{2}(\boldsymbol{a}\otimes\boldsymbol{b}-\boldsymbol{b}\otimes\boldsymbol{a})\boldsymbol{c}\\&=\frac{1}{2}\left((\boldsymbol{b}\cdot\boldsymbol{c})\boldsymbol{a}-(\boldsymbol{a}\cdot\boldsymbol{c})\boldsymbol{b}\right)\\&=\frac{1}{2}(\boldsymbol{b}\times\boldsymbol{a})\times\boldsymbol{c}\end{aligned}$$

we have

$$\text{vect}(\boldsymbol{a}\otimes\boldsymbol{b})=\frac{1}{2}(\boldsymbol{b}\times\boldsymbol{a}) \tag{136}$$

Accordingly,

$$2\text{vect}\big(\ddot{\boldsymbol{F}}\boldsymbol{E}_0\boldsymbol{F}^T\big)=2\text{vect}\big(E_0^{ij}\ddot{\boldsymbol{d}}_i\otimes\boldsymbol{d}_j\big)=E_0^{ij}\boldsymbol{d}_j\times\ddot{\boldsymbol{d}}_i \tag{137}$$

$$2\text{vect}\big(\boldsymbol{M}_{\text{ext}}\boldsymbol{F}^T\big)=2\text{vect}\big(\boldsymbol{f}^i_{\text{ext}}\otimes\boldsymbol{d}_i\big)=\boldsymbol{d}_i\times\boldsymbol{f}^i_{\text{ext}}=\overline{\boldsymbol{m}}_{\text{ext}} \tag{138}$$

A.1.1 Balance of Angular Momentum

To get the balance law for angular momentum, substitute $\delta\boldsymbol{U}=\boldsymbol{0}$ into (134), $\boldsymbol{\omega}_\delta=\boldsymbol{\xi}$ into (135), and $\delta\overline{\boldsymbol{x}}=\boldsymbol{\xi}\times\overline{\boldsymbol{x}}$ into (130). Subsequent summation of the resulting equations yields

$$\boldsymbol{\xi}\cdot\left(M\overline{\boldsymbol{x}}\times\ddot{\overline{\boldsymbol{x}}}+2\text{vect}\big(\ddot{\boldsymbol{F}}\boldsymbol{E}_0\boldsymbol{F}^T\big)-\overline{\boldsymbol{x}}\times\boldsymbol{f}_{\text{ext}}-2\text{vect}\big(\boldsymbol{M}_{\text{ext}}\boldsymbol{F}^T\big)\right)=0$$

or

$$\boldsymbol{\xi}\cdot\left(\frac{d}{dt}\boldsymbol{j}-\boldsymbol{m}_{\text{ext}}\right)=0$$

The last equation has to hold for arbitrary $\boldsymbol{\xi}\in\mathbb{R}^3$. Accordingly, one obtains $d\boldsymbol{j}/dt=\boldsymbol{m}_{\text{ext}}$, where

$$\begin{aligned}\boldsymbol{j}&=M\overline{\boldsymbol{x}}\times\dot{\overline{\boldsymbol{x}}}+2\text{vect}\big(\dot{\boldsymbol{F}}\boldsymbol{E}_0\boldsymbol{F}^T\big)\\\boldsymbol{m}_{\text{ext}}&=\overline{\boldsymbol{x}}\times\boldsymbol{f}_{\text{ext}}+2\text{vect}\big(\boldsymbol{M}_{\text{ext}}\boldsymbol{F}^T\big)\end{aligned}$$

denote, respectively, the total angular momentum and the resultant external torque with respect to the origin of the inertial frame of reference. Note that the same conclusions can be drawn by substituting $\delta\overline{\boldsymbol{x}} = \boldsymbol{\xi} \times \overline{\boldsymbol{x}}$ into (130), and $\delta\boldsymbol{F} = \widehat{\boldsymbol{\xi}}\boldsymbol{F}$ into (131).

A.1.2 Balance of Energy

Suppose that an external force $\boldsymbol{f}_{\text{ext}} \in \mathbb{R}^3$ along with external director forces $\boldsymbol{f}^i_{\text{ext}} \in \mathbb{R}^3$, $i = 1, 2, 3$, are acting on the body under consideration. Recall that the external director forces $\boldsymbol{f}^i_{\text{ext}}$ can be linked to the second-order tensor $\boldsymbol{M}_{\text{ext}}$ via $\boldsymbol{M}_{\text{ext}} = \boldsymbol{f}^i_{\text{ext}} \otimes \boldsymbol{D}_i$ (see Eq. (38) in Sect. 2.2). To define the external director forces we introduce 9 independent quantities $\mathcal{M}^{ij}$ such that

$$\boldsymbol{\mathcal{M}} = \mathcal{M}^{ij}\boldsymbol{D}_i \otimes \boldsymbol{D}_j \tag{139}$$

and

$$\boldsymbol{M}_{\text{ext}} = \boldsymbol{F}\boldsymbol{\mathcal{M}} = \mathcal{M}^{ij}\boldsymbol{d}_i \otimes \boldsymbol{D}_j \tag{140}$$

Note that the last equation implies

$$\boldsymbol{f}^i_{\text{ext}} = \mathcal{M}^{ki}\boldsymbol{d}_k \tag{141}$$

Now substitute $\dot{\overline{\boldsymbol{x}}}$ for $\delta\overline{\boldsymbol{x}}$ into (130) and $\dot{\boldsymbol{F}}$ for $\delta\boldsymbol{F}$ into (131). Subsequent summation of both equations yields

$$\dot{\overline{\boldsymbol{x}}} \cdot \left(M\ddot{\overline{\boldsymbol{x}}} - \boldsymbol{f}_{\text{ext}}\right) + \text{tr}\left(\dot{\boldsymbol{F}}^T\left(\ddot{\boldsymbol{F}}\boldsymbol{E}_0 + 2\boldsymbol{F}DU(\boldsymbol{C}) - \boldsymbol{M}_{\text{ext}}\right)\right) = 0 \tag{142}$$

Taking into account the relationships

$$\dot{\overline{\boldsymbol{x}}} \cdot M\ddot{\overline{\boldsymbol{x}}} = \frac{d}{dt}\left(\frac{1}{2}M\dot{\overline{\boldsymbol{x}}} \cdot \dot{\overline{\boldsymbol{x}}}\right)$$
$$\text{tr}\left(\dot{\boldsymbol{F}}^T\ddot{\boldsymbol{F}}\boldsymbol{E}_0\right) = \frac{d}{dt}\left(\frac{1}{2}\text{tr}\left(\dot{\boldsymbol{F}}^T\dot{\boldsymbol{F}}\boldsymbol{E}_0\right)\right)$$

we define the kinetic energy

$$T = \frac{1}{2}M\dot{\overline{\boldsymbol{x}}} \cdot \dot{\overline{\boldsymbol{x}}} + \frac{1}{2}\text{tr}\left(\dot{\boldsymbol{F}}\boldsymbol{E}_0\dot{\boldsymbol{F}}^T\right) \tag{143}$$

Moreover,

$$\begin{aligned}\text{tr}\left(\dot{\boldsymbol{F}}^T\boldsymbol{F}2DU(\boldsymbol{C})\right) &= \text{tr}\left(2DU(\boldsymbol{C})\text{sym}(\dot{\boldsymbol{F}}^T\boldsymbol{F})\right)\\ &= \text{tr}\left(2DU(\boldsymbol{C})\frac{1}{2}(\dot{\boldsymbol{F}}^T\boldsymbol{F}+\boldsymbol{F}^T\dot{\boldsymbol{F}})\right)\\ &= \text{tr}\left(2DU(\boldsymbol{C})\frac{1}{2}\dot{\boldsymbol{C}}\right)\\ &= \frac{d}{dt}U(\boldsymbol{C})\end{aligned}$$

Now (142) can be recast in the form

$$\frac{d}{dt}E = P_{\text{ext}} \tag{144}$$

Here, E is the total mechanical energy given by

$$E = T + U$$

where U denotes the total strain energy defined in (13). On the right hand side of balance equation (144)

$$P_{\text{ext}} = \boldsymbol{f}_{\text{ext}}\cdot\dot{\bar{\boldsymbol{x}}} + \text{tr}\left(\dot{\boldsymbol{F}}^T\boldsymbol{M}_{\text{ext}}\right)$$

denotes the power of the external forces acting on the pseudo-rigid body. We next focus on the power of the director forces given by

$$\overline{P}_{\text{ext}} = \text{tr}\left(\dot{\boldsymbol{F}}^T\boldsymbol{M}_{\text{ext}}\right)$$

Taking into account (140), the last equation can be rewritten as

$$\begin{aligned}\overline{P}_{\text{ext}} &= \text{tr}\left(\dot{\boldsymbol{F}}^T\boldsymbol{F}\boldsymbol{\mathcal{M}}\right)\\ &= \text{tr}\left((\overline{\boldsymbol{\mathcal{M}}}+\widetilde{\boldsymbol{\mathcal{M}}})\dot{\boldsymbol{F}}^T\boldsymbol{F}\right)\end{aligned}$$

In the last equation

$$\begin{aligned}\overline{\boldsymbol{\mathcal{M}}} &= \text{sym}\,(\boldsymbol{\mathcal{M}})\\ \widetilde{\boldsymbol{\mathcal{M}}} &= \text{skew}\,(\boldsymbol{\mathcal{M}})\end{aligned}$$

have been introduced. Now

$$\text{tr}\left(\overline{\boldsymbol{\mathcal{M}}}\dot{\boldsymbol{F}}^T\boldsymbol{F}\right) = \text{tr}\left(\overline{\boldsymbol{\mathcal{M}}}\text{sym}\left(\dot{\boldsymbol{F}}^T\boldsymbol{F}\right)\right) = \frac{1}{2}\text{tr}\left(\overline{\boldsymbol{\mathcal{M}}}\dot{\boldsymbol{C}}\right)$$

Furthermore,

$$\operatorname{tr}\left(\widetilde{\mathcal{M}}\dot{\boldsymbol{F}}^T\boldsymbol{F}\right) = \operatorname{tr}\left(\widetilde{\mathcal{M}}\operatorname{skew}\left(\dot{\boldsymbol{F}}^T\boldsymbol{F}\right)\right)$$

Applying the polar decomposition $\boldsymbol{F} = \boldsymbol{R}\boldsymbol{U}$ along with $\dot{\boldsymbol{F}} = \dot{\boldsymbol{R}}\boldsymbol{U} + \boldsymbol{R}\dot{\boldsymbol{U}}$ and $\widehat{\boldsymbol{\omega}} = \dot{\boldsymbol{R}}\boldsymbol{R}^T$ (cf. (132) and (133) on p. 47), we get

$$\operatorname{tr}\left(\widetilde{\mathcal{M}}\operatorname{skew}\left(\dot{\boldsymbol{F}}^T\boldsymbol{F}\right)\right) = \boldsymbol{\omega}\cdot 2\operatorname{vect}\left(\boldsymbol{F}\widetilde{\mathcal{M}}\boldsymbol{F}^T\right) + \operatorname{tr}\left(\widetilde{\mathcal{M}}\dot{\boldsymbol{U}}^T\boldsymbol{U}\right)$$

Altogether the power of the external forces can be written in the form

$$\begin{aligned} P_{\text{ext}} &= \boldsymbol{f}_{\text{ext}}\cdot\dot{\bar{\boldsymbol{x}}} + \frac{1}{2}\operatorname{tr}\left(\overline{\mathcal{M}}\dot{\boldsymbol{C}}\right) + \boldsymbol{\omega}\cdot 2\operatorname{vect}\left(\boldsymbol{F}\widetilde{\mathcal{M}}\boldsymbol{F}^T\right) + \operatorname{tr}\left(\widetilde{\mathcal{M}}\dot{\boldsymbol{U}}^T\boldsymbol{U}\right) \\ &= \boldsymbol{f}_{\text{ext}}\cdot\dot{\bar{\boldsymbol{x}}} + \frac{1}{2}\overline{\mathcal{M}}^{ij}\dot{d}_{ij} + \boldsymbol{\omega}\cdot\overline{\boldsymbol{m}}_{\text{ext}} + \operatorname{tr}\left(\widetilde{\mathcal{M}}\dot{\boldsymbol{U}}^T\boldsymbol{U}\right) \end{aligned}$$

Here, $\overline{\boldsymbol{m}}_{\text{ext}}$ can be identified as the resultant external torque relative to the center of mass that has been introduced in (71). In particular, we have

$$\begin{aligned} \overline{\boldsymbol{m}}_{\text{ext}} &= 2\operatorname{vect}\left(\boldsymbol{F}\widetilde{\mathcal{M}}\boldsymbol{F}^T\right) \\ &= \widetilde{\mathcal{M}}^{ji}\boldsymbol{d}_i\times\boldsymbol{d}_j \\ &= \varepsilon_{ijk}\widetilde{\mathcal{M}}^{ji}\boldsymbol{d}^k \\ &= \boldsymbol{d}_i\times\boldsymbol{f}^i_{\text{ext}} \end{aligned}$$

In the last equation use has been made of (141). Moreover,

$$\varepsilon_{ijk} = (\boldsymbol{d}_i\times\boldsymbol{d}_j)\cdot\boldsymbol{d}_k = e_{ijk}\sqrt{d}$$

where $d = \det(d_{ij})$ (or $\sqrt{d} = (\boldsymbol{d}_1\times\boldsymbol{d}_2)\cdot\boldsymbol{d}_3$) and e_{ijk} denotes the alternating symbol.

A.2 Application of External Torques

It can be observed from the above treatment that the application of external torques $\overline{\boldsymbol{m}}_{\text{ext}}$ relative to the center of mass is linked to the skew-symmetric tensor $\widetilde{\mathcal{M}} = \widetilde{\mathcal{M}}^{ij}\boldsymbol{D}_i\otimes\boldsymbol{D}_j$. In particular, given the covariant components of the external torque, $m_k = \boldsymbol{d}_k\cdot\overline{\boldsymbol{m}}_{\text{ext}}$, we obtain

$$m_k = \varepsilon_{ijk}\widetilde{\mathcal{M}}^{ji}$$

from which it follows that

$$\widetilde{\mathcal{M}}^{23} = -\widetilde{\mathcal{M}}^{32} = -\frac{m_1}{2\sqrt{d}}$$
$$\widetilde{\mathcal{M}}^{31} = -\widetilde{\mathcal{M}}^{13} = -\frac{m_2}{2\sqrt{d}}$$
$$\widetilde{\mathcal{M}}^{12} = -\widetilde{\mathcal{M}}^{21} = -\frac{m_3}{2\sqrt{d}}$$

or

$$\widetilde{\mathcal{M}}^{ij} = \frac{e^{jik} m_k}{2\sqrt{d}} \tag{145}$$

where $e^{ijk} = e_{ijk}$ again denotes the alternating symbol. Accordingly, using the above formulas for $\widetilde{\mathcal{M}}^{ij}$ in terms of the torque components m_k, the corresponding director forces can be calculated via

$$\boldsymbol{f}^j_{\text{ext}} = \widetilde{\mathcal{M}}^{ij} \boldsymbol{d}_i \tag{146}$$

or

$$\boldsymbol{f}^j_{\text{ext}} = \frac{e^{ijk}}{2\sqrt{d}} \left(\boldsymbol{d}_j \otimes \boldsymbol{d}_k \right) \overline{\boldsymbol{m}}_{\text{ext}} \tag{147}$$

To summarize, the action of an external torque $\overline{\boldsymbol{m}}_{\text{ext}}$ relative to the center of mass can be realized by applying external director forces of the form

$$\begin{bmatrix} \boldsymbol{f}^1_{\text{ext}} \\ \boldsymbol{f}^2_{\text{ext}} \\ \boldsymbol{f}^3_{\text{ext}} \end{bmatrix} = \frac{1}{2\sqrt{d}} \begin{bmatrix} \boldsymbol{d}_2 \otimes \boldsymbol{d}_3 - \boldsymbol{d}_3 \otimes \boldsymbol{d}_2 \\ \boldsymbol{d}_3 \otimes \boldsymbol{d}_1 - \boldsymbol{d}_1 \otimes \boldsymbol{d}_3 \\ \boldsymbol{d}_1 \otimes \boldsymbol{d}_2 - \boldsymbol{d}_2 \otimes \boldsymbol{d}_1 \end{bmatrix} \overline{\boldsymbol{m}}_{\text{ext}} \tag{148}$$

Remark A.1 Formula (148) can be viewed as an extension to flexible Cosserat points of the method proposed in Betsch and Sänger (2013). In this work the consistent application of torques has been dealt with in the context of rigid body dynamics formulated in terms of directors (or direction cosines). The formula proposed in Betsch and Sänger (2013) is given by

$$\boldsymbol{f}^j_{\text{ext}} = \frac{1}{2} \overline{\boldsymbol{m}}_{\text{ext}} \times \boldsymbol{d}^j \tag{149}$$

The equivalence of (149) to (148) can be shown by a direct calculation:

$$\begin{aligned} \boldsymbol{f}^j_{\text{ext}} &= \frac{1}{2}\overline{\boldsymbol{m}}_{\text{ext}} \times \boldsymbol{d}^j \\ &= \frac{1}{2} m_k \boldsymbol{d}^k \times \boldsymbol{d}^j \\ &= \frac{1}{2} m_k d^{-\frac{1}{2}} e^{kji} \boldsymbol{d}_i \\ &= \widetilde{\mathcal{M}}^{ij} \boldsymbol{d}_i \end{aligned}$$

where (145) has been used.

A.2.1 Fully Actuated Cosserat Point

If the Cosserat point shall be fully actuated, the 9 independent quantities $\mathcal{M}^{ij}$ in (139) can be employed as control inputs. According to (141) this approach determines the external director forces

$$\boldsymbol{f}^i_{\text{ext}} = \mathcal{M}^{ji} \boldsymbol{d}_j$$

If required the external torque associated with the control inputs can be extracted via

$$\overline{\boldsymbol{m}}_{\text{ext}} = \mathcal{M}^{ji} \boldsymbol{d}_i \times \boldsymbol{d}_j$$

Note that due to the presence of the cross product the skew-symmetric part of $\mathcal{M}^{ji}$, that is, $\widetilde{\mathcal{M}}^{ji} = (\mathcal{M}^{ji} - \mathcal{M}^{ij})/2$, is automatically extracted. The above result coincides with

$$\overline{\boldsymbol{m}}_{\text{ext}} = m_k \boldsymbol{d}^k \quad \text{where} \quad m_k = \sqrt{d}\, e_{ijk} \mathcal{M}^{ji}$$

Again the skew-symmetric part of $\mathcal{M}^{ji}$ is extracted due to the presence of the alternating symbol.

A.3 Iteration Matrix of the EM Integrator

Consider St. Venant-Kirchhoff material with strain energy density

$$W(\boldsymbol{G}) = \frac{\lambda}{2} (\text{tr}\boldsymbol{G})^2 + \mu \text{tr}\left(\boldsymbol{G}^2\right)$$

where the Green–Lagrangean strain tensor is given by

$$\boldsymbol{G} = \frac{1}{2}(\boldsymbol{C} - \boldsymbol{I}) = \gamma_{ij} \boldsymbol{D}^i \otimes \boldsymbol{D}^j$$

Note that the components $\gamma_{ij} = \frac{1}{2}(d_{ij} - \delta_{ij})$ have been introduced in (66). According to (11), the second Piola-Kirchhoff stress tensor is given by

$$\begin{aligned} \boldsymbol{S} &= 2DW(\boldsymbol{C}) \\ &= DW(\boldsymbol{G}) \\ &= \lambda\,(\mathrm{tr}\boldsymbol{G})\,\boldsymbol{I} + 2\mu\boldsymbol{G} \end{aligned} \tag{150}$$

Moreover, the fourth-order elasticity tensor assumes the form

$$\begin{aligned} \mathsf{C} &= 4D^2W(\boldsymbol{C}) \\ &= D^2W(\boldsymbol{G}) \\ &= \lambda\boldsymbol{I}\otimes\boldsymbol{I} + 2\mu\mathbf{I} \end{aligned} \tag{151}$$

Since we have assumed that the director triad $\{\boldsymbol{D}_i\}$ in the reference configuration is orthonormal, it suffices to consider the Cartesian components of $\boldsymbol{S}$ and C. Accordingly, we have

$$S_{ij} = \lambda\gamma_{kk}\delta_{ij} + 2\mu\gamma_{ij} \tag{152}$$

and

$$\mathsf{C}_{ijkl} = \lambda\delta_{ij}\delta_{kl} + \mu\left(\delta_{ik}\delta_{jl} + \delta_{il}\delta_{jk}\right)$$

We next deal with the linearization of the internal director forces $\boldsymbol{f}^i_{\mathrm{int}} = S^{ij}\boldsymbol{d}_j$. First consider the time-continuous case where, according to the product rule of differentiation, we get

$$\Delta\boldsymbol{f}^i_{\mathrm{int}} = \Delta S^{ij}\boldsymbol{d}_j + S^{ij}\Delta\boldsymbol{d}_j \tag{153}$$

With regard to (152)

$$\begin{aligned} \Delta S_{ij} &= \lambda\Delta\gamma_{kk}\delta_{ij} + 2\mu\Delta\gamma_{ij} \\ &= \lambda(\boldsymbol{d}_k\cdot\Delta\boldsymbol{d}_k)\delta_{ij} + \mu(\boldsymbol{d}_i\cdot\Delta\boldsymbol{d}_j + \boldsymbol{d}_j\cdot\Delta\boldsymbol{d}_i) \end{aligned} \tag{154}$$

Now, a straightforward calculation yields

$$\Delta\boldsymbol{f}^i_{\mathrm{int}} = \left(\boldsymbol{K}^{ij}_{\mathrm{mat}} + \boldsymbol{K}^{ij}_{\mathrm{geo}}\right)\Delta\boldsymbol{d}_j \tag{155}$$

where the contributions to the iteration matrix have been split into a material part $\boldsymbol{K}^{ij}_{\mathrm{mat}}$ and a geometric part $\boldsymbol{K}^{ij}_{\mathrm{geo}}$. The material part is given by

$$\boldsymbol{K}^{ij}_{\mathrm{mat}} = \lambda\boldsymbol{d}_i\otimes\boldsymbol{d}_j + \mu\boldsymbol{d}_j\otimes\boldsymbol{d}_i + \mu\boldsymbol{d}_k\otimes\boldsymbol{d}_k\,\delta_{ij}$$

and the geometric part assumes the form

$$\boldsymbol{K}^{ij}_{\mathrm{geo}} = S_{ij}\boldsymbol{I}$$

The symmetry of the iteration matrix follows from the properties $\boldsymbol{K}^{ij}_{\text{mat}} = (\boldsymbol{K}^{ji}_{\text{mat}})^T$ and $\boldsymbol{K}^{ij}_{\text{geo}} = (\boldsymbol{K}^{ji}_{\text{geo}})^T$. Similar to (153), in the discrete case the EM scheme (63) leads to

$$\Delta\ (\boldsymbol{f}^i_{\text{int}})\big|_{n+\frac{1}{2}} = \Delta S^{ij}_A \boldsymbol{d}_{j_{n+\frac{1}{2}}} + S^{ij}_A \Delta \boldsymbol{d}_{j_{n+\frac{1}{2}}}$$

Similar to (154), the algorithmic stress formula (65) leads to

$$\begin{aligned} \Delta S^{ij}_A &= \lambda \Delta \gamma_{kk_{n+\frac{1}{2}}}\, \delta_{ij} + 2\mu \Delta \gamma_{ij_{n+\frac{1}{2}}} \\ &= \tfrac{\lambda}{2}(\boldsymbol{d}_{k_{n+1}} \cdot \Delta \boldsymbol{d}_{k_{n+1}})\delta_{ij} + \tfrac{\mu}{2}(\boldsymbol{d}_{i_{n+1}} \cdot \Delta \boldsymbol{d}_{j_{n+1}} + \boldsymbol{d}_{j_{n+1}} \cdot \Delta \boldsymbol{d}_{i_{n+1}}) \end{aligned} \tag{156}$$

Altogether the discrete counterpart of (155) is given by the consistent linearization

$$\Delta\ (\boldsymbol{f}^i_{\text{int}})\big|_{n+\frac{1}{2}} = \left(\boldsymbol{K}^{ij}_{\text{mat}}\Big|_{n+\frac{1}{2}} + \boldsymbol{K}^{ij}_{\text{geo}}\Big|_{n+\frac{1}{2}} \right) \Delta \boldsymbol{d}_{j_{n+1}}$$

where the material part is given by

$$\boldsymbol{K}^{ij}_{\text{mat}}\Big|_{n+\frac{1}{2}} = \frac{1}{2}\left(\lambda \boldsymbol{d}_{i_{n+\frac{1}{2}}} \otimes \boldsymbol{d}_{j_{n+1}} + \mu \boldsymbol{d}_{j_{n+\frac{1}{2}}} \otimes \boldsymbol{d}_{i_{n+1}} + \mu \boldsymbol{d}_{k_{n+\frac{1}{2}}} \otimes \boldsymbol{d}_{k_{n+1}}\, \delta_{ij} \right)$$

and the geometric part assumes the form

$$\boldsymbol{K}^{ij}_{\text{geo}}\Big|_{n+\frac{1}{2}} = \frac{1}{2} S^{ij}_A \boldsymbol{I}$$

It is obvious that in the discrete setting the material part destroys the symmetry of the iteration matrix, for

$$\left(\boldsymbol{K}^{ij}_{\text{mat}}\right)\Big|_{n+\frac{1}{2}} \neq \left(\boldsymbol{K}^{ji}_{\text{mat}}\right)^T\Big|_{n+\frac{1}{2}}$$

We finally remark that due to definition (13) of the total strain energy of the Cosserat point, namely $U(\boldsymbol{C}) = V_0 W(\boldsymbol{C})$, the above stress components S^{ij} should be replaced by $\overline{S}^{ij} = V_0 S^{ij}$.

References

Antman, S. S. (2005). *Nonlinear problems of elasticity* (2nd ed.). Springer.

Armero, F., & Petöcz, E. (1998). Formulation and analysis of conserving algorithms for frictionless dynamic contact/impact problems. *Computer Methods in Applied Mechanics and Engineering*, *158*, 269–300.

Armero, F., & Romero, I. (2001). On the formulation of high-frequency dissipative time-stepping algorithms for nonlinear dynamics. Part II: Second-order methods. *Computer Methods in Applied Mechanics and Engineering*, *190*, 6783–6824.

Armero, F., & Romero, I. (2003). Energy-dissipative momentum-conserving time-stepping algorithms for the dynamics of nonlinear Cosserat rods. *Computational Mechanics*, *31*, 3–26.

Ascher, U. M., & Petzold, L. R. (1998). Computer methods for ordinary differential equations and differential-algebraic equations. SIAM.

Bauchau, O. A. (2011). *Flexible multibody dynamics*. Solid mechanics and its applications New York: Springer.

Bauchau, O. A., & Bottasso, C. L. (1999). On the design of energy preserving and decaying schemes for flexible, nonlinear multi-body systems. *Computer Methods in Applied Mechanics and Engineering*, *169*(1–2), 61–79.

Betsch, P. (2006). Energy-consistent numerical integration of mechanical systems with mixed holonomic and nonholonomic constraints. *Computer Methods in Applied Mechanics and Engineering*, *195*, 7020–7035.

Betsch, P., & Leyendecker, S. (2006). The discrete null space method for the energy consistent integration of constrained mechanical systems. Part II: Multibody dynamics. *International Journal for Numerical Methods in Engineering*, *67*(4), 499–552.

Betsch, P., & Sänger, N. (2009a). On the use of geometrically exact shells in a conserving framework for flexible multibody dynamics. *Computer Methods in Applied Mechanics and Engineering*, *198*, 1609–1630.

Betsch, P., & Sänger, N. (2009b). A nonlinear finite element framework for flexible multibody dynamics: Rotationless formulation and energy-momentum conserving discretization. In C. L. Bottasso (Ed.), *Multibody Dynamics: Computational Methods and Applications, Computational Methods in Applied Sciences* (Vol. 12, pp. 119–141). Springer.

Betsch, P., & Sänger, N. (2013). On the consistent formulation of torques in a rotationless framework for multibody dynamics. *Computers & Structures*, *127*, 29–38.

Betsch, P., & Steinmann, P. (2002a). Conservation properties of a time FE method. Part III: Mechanical systems with holonomic constraints. *International Journal for Numerical Methods in Engineering*, *53*, 2271–2304.

Betsch, P., & Steinmann, P. (2002b). Frame-indifferent beam finite elements based upon the geometrically exact beam theory. *International Journal for Numerical Methods in Engineering*, *54*, 1775–1788.

Betsch, P., & Steinmann, P. (2002c). A DAE approach to flexible multibody dynamics. *Multibody System Dynamics*, *8*, 367–391.

Betsch, P., & Steinmann, P. (2003). Constrained dynamics of geometrically exact beams. *Computational Mechanics*, *31*, 49–59.

Betsch, P., & Uhlar, S. (2007). Energy-momentum conserving integration of multibody dynamics. *Multibody System Dynamics*, *17*(4), 243–289.

Betsch, P., Hesch, C., Sänger, N., & Uhlar, S. (2010). Variational integrators and energy-momentum schemes for flexible multibody dynamics. *Journal of Computational and Nonlinear Dynamics*, *5*(3), 031001/1-11.

Betsch, P., Siebert, R., & Sänger, N. (2012). Natural coordinates in the optimal control of multibody systems. *Journal of Computational and Nonlinear Dynamics*, *7*(1), 011009/1-8.

Bottasso, C. L., & Croce, A. (2004). Optimal control of multibody systems using an energy preserving direct transcription method. *Multibody System Dynamics*, *12*(1), 17–45.

Bottasso, C. L., & Trainelli, L. (2004). An attempt at the classification of energy decaying schemes for structural and multibody dynamics. *Multibody System Dynamics*, *12*(2), 173–185.

Bottasso, C. L., Borri, M., & Trainelli, L. (2001). Integration of elastic multibody systems by invariant conserving/dissipating algorithms. II. Numerical schemes and applications. *Computer Methods in Applied Mechanics and Engineering*, *190*, 3701–3733.

Bottasso, C. L., Bauchau, O. A., & Choi, J.-Y. (2002). An energy decaying scheme for nonlinear dynamics of shells. *Computer Methods in Applied Mechanics and Engineering*, *191*(27–28), 3099–3121.

Bottema, O., & Roth, B. (1979). *Theoretical Kinematics*. Amsterdam: North-Holland Publishing Company.

Brank, B., Briseghella, L., Tonello, N., & Damjanic, F. B. (1998). On non-linear dynamics of shells: Implementation of energy-momentum conserving algorithm for a finite rotation shell model. *International Journal for Numerical Methods in Engineering*, *42*, 409–442.

Cohen, H., & Muncaster, R. G. (1988). *The theory of Pseudo-rigid Bodies*. New York: Springer.

Conde Martín, S., Betsch, P., & García Orden, J. C. (2016). A temperature-based thermodynamically consistent integration scheme for discrete thermo-elastodynamics. *Communications in Nonlinear Science and Numerical Simulation*, *32*, 63–80.

Crisfield, M. A. (1997). *Non-linear finite element analysis of solids and structures*. Advanced topics. New York: Wiley.

Crisfield, M. A., & Shi, J. (1994). A co-rotational element/time-integration strategy for non-linear dynamics. *International Journal for Numerical Methods in Engineering*, *37*, 1897–1913.

de García Jalón, J. (2007). Twenty-five years of natural coordinates. *Multibody System Dynamics*, *18*(1), 15–33.

de Jalón, J. G., & Bayo, E. (1994). *Kinematic and dynamic simulation of multibody systems: The real-time challenge*. Springer.

Géradin, M. G., & Cardona, A. (2001). *Flexible multibody dynamics: A finite element approach*. Wiley.

Gonzalez, O. (1996). Time integration and discrete Hamiltonian systems. *Journal of Nonlinear Science*, *6*, 449–467.

Gonzalez, O., & Simo, J. C. (1996). On the stability of symplectic and energy-momentum algorithms for non-linear Hamiltonian systems with symmetry. *Computer Methods in Applied Mechanics and Engineering*, *134*, 197–222.

Greenspan, D. (1984). Conservative numerical methods for $\ddot{x} = f(x)$. *Journal of Computational Physics*, *56*, 28–41.

Groß, M., & Betsch, P. (2011). Galerkin-based energy-momentum consistent time-stepping algorithms for classical nonlinear thermo-elastodynamics. *Mathematics and Computers in Simulation*, *82*(4), 718–770.

Groß, M., & Betsch, P. (2010). Energy-momentum consistent finite element discretization of dynamic finite viscoelasticity. *International Journal for Numerical Methods in Engineering*, *81*(11), 1341–1386.

Groß, M., Betsch, P., & Steinmann, P. (2005). Conservation properties of a time FE method. Part IV: Higher order energy and momentum conserving. *International Journal for Numerical Methods in Engineering*, *63*, 1849–1897.

Gurtin, M. E. (1981). *An introduction to continuum mechanics*. Academic Press.

Hesch, C., & Betsch, P. (2011a). Transient 3d contact problems-NTS method: mixed methods and conserving integration. *Computational Mechanics*, *48*(4), 437–449.

Hesch, C., & Betsch, P. (2010). Transient three-dimensional domain decomposition problems: Frame-indifferent mortar constraints and conserving integration. *International Journal for Numerical Methods in Engineering*, *82*(3), 329–358.

Hesch, C., & Betsch, P. (2011b). Transient three-dimensional contact problems: mortar method. Mixed methods and conserving integration. *Computational Mechanics*, *48*(4), 461–475.

Hesch, C., & Betsch, P. (2009). A mortar method for energy-momentum conserving schemes in frictionless dynamic contact problems. *International Journal for Numerical Methods in Engineering*, *77*(10), 1468–1500.

Hesch, C., & Betsch, P. (2011c). Energy-momentum consistent algorithms for dynamic thermomechanical problems—application to mortar domain decomposition problems. *International Journal for Numerical Methods in Engineering*, *86*(11), 1277–1302.

Hughes, T. J. R. (2000). *The Finite element method*. Dover Publications.

Hughes, T. J. R., & Winget, J. (1980). Finite rotation effects in numerical integration of rate constitutive equations arising in large-deformation analysis. *International Journal for Numerical Methods in Engineering*, *15*, 1862–1867.

Hughes, T. J. R., Caughey, T. K., & Liu, W. K. (1978). Finite-element methods for nonlinear elastodynamics which conserve energy. *Journal of Applied Mechanics*, *45*, 366–370.

Ibrahimbegović, A. (2009). *Nonlinear solid mechanics. Solid mechanics and its applications* (Vol. 160). Springer.

Ibrahimbegović, A., Mamouri, S., Taylor, R. L., & Chen, A. J. (2000). Finite element method in dynamics of flexible multibody systems: Modeling of holonomic constraints and energy conserving integration schemes. *Multibody System Dynamics*, *4*(2–3), 195–223.

Johnson, E. R., & Murphey, T. D. (2009). Scalable variational integrators for constrained mechanical systems in generalized coordinates. *IEEE Transactions on Robotics*, *25*(6), 1249–1261.

Koch, M. W., & Leyendecker, S. (2013). Energy momentum consistent force formulation for the optimal control of multibody systems. *Multibody System Dynamics*, *29*, 381–401.

Krenk, S. (2009). *Non-linear modeling and analysis of solids and structures*. Cambridge University Press.

Kuhl, D., & Crisfield, M. A. (1999). Energy-conserving and decaying algorithms in non-linear structural mechanics. *International Journal for Numerical Methods in Engineering*, *45*, 569–599.

Kunkel, P., & Mehrmann, V. (2006). *Differential-algebraic equations*. European Mathematical Society.

Laursen, T. A. (2002). *Computational contact and impact mechanics*. Springer.

Laursen, T. A., & Chawla, V. (1997). Design of energy conserving algorithms for frictionless dynamic contact problems. *International Journal for Numerical Methods in Engineering*, *40*, 863–886.

Lens, E., & Cardona, A. (2007). An energy preserving/decaying scheme for nonlinearly constrained multibody systems. *Multibody System Dynamics*, *18*(3), 435–470.

Lens, E. V., Cardona, A., & Géradin, M. (2004). Energy preserving time integration for constrained multibody systems. *Multibody System Dynamics*, *11*(1), 41–61.

Lewis, D., & Simo, J. C. (1994). Conserving algorithms for the dynamics of Hamiltonian systems on Lie groups. *Journal of Nonlinear Science*, *4*, 253–299.

Leyendecker, S., Betsch, P., & Steinmann, P. (2006). Objective energy-momentum conserving integration for the constrained dynamics of geometrically exact beams. *Computer Methods in Applied Mechanics and Engineering*, *195*, 2313–2333.

Leyendecker, S., Betsch, P., & Steinmann, P. (2008a). The discrete null space method for the energy consistent integration of constrained mechanical systems. Part III: Flexible multibody dynamics. *Multibody System Dynamics*, *19*(1–2), 45–72.

Leyendecker, S., Marsden, J. E., & Ortiz, M. (2008b). Variational integrators for constrained dynamical systems. *Zeitschrift für Angewandte Mathematik und Mechanik (ZAMM)*, *88*(9), 677–708.

Leyendecker, S., Ober-Blöbaum, S., Marsden, J. E., & Ortiz, M. (2010). Discrete mechanics and optimal control for constrained systems. *Optimal Control Applications and Methods*, *31*(6), 505–528.

Marsden, J. E., & Ratiu, T. S. (1999). *Introduction to mechanics and symmetry* (2nd ed.). Springer.

McPhee, J. J., & Redmond, S. M. (2006). Modelling multibody systems with indirect coordinates. *Computer Methods in Applied Mechanics and Engineering*, *195*, 6942–6957.

Nordenholz, T. R., & O'Reilly, O. M. (1998). On steady motions of isotropic, elastic Cosserat points. *IMA Journal of Applied Mathematics*, *60*, 55–72.

Ober-Blöbaum, S., Junge, O., & Marsden, J. E. (2011). Discrete mechanics and optimal control: An analysis. *ESAIM: Control, Optimisation and Calculus of Variations*, *17*(2), 322–352.

Romero, I. (2009). Thermodynamically consistent time-stepping algorithms for non-linear thermomechanical systems. *International Journal for Numerical Methods in Engineering*, *79*(6), 706–732.

Romero, I. (2010). Algorithms for coupled problems that preserve symmetries and the laws of thermodynamics: Part II: Fractional step methods. *Computer Methods in Applied Mechanics and Engineering*, *199*(33–36), 2235–2248.

Romero, I. (2012). An analysis of the stress formula for energy-momentum methods in nonlinear elastodynamics. *Computational Mechanics*, *50*, 603–610.

Romero, I., & Armero, F. (2002a). An objective finite element approximation of the kinematics of geometrically exact rods and its use in the formulation of an energy-momentum conserving scheme in dynamics. *International Journal for Numerical Methods in Engineering*, *54*, 1683–1716.

Romero, I., & Armero, F. (2002b). Numerical integration of the stiff dynamics of geometrically exact shells: an energy-dissipative momentum-conserving scheme. *International Journal for Numerical Methods in Engineering*, *54*, 1043–1086.

Rubin, M. B. (2000). *Cosserat theories: shells, rods and points, solid mechanics and its applications* (Vol. 79). Kluwer Academic Publishers.

Simo, J. C., & Tarnow, N. (1992). The discrete energy-momentum method. Conserving algorithms for nonlinear elastodynamics. *Zeitschrift für angewandte Mathematik und Physik (ZAMP)*, *43*, 757–792.

Simo, J. C., & Tarnow, N. (1994). A new energy and momentum conserving algorithm for the nonlinear dynamics of shells. *International Journal for Numerical Methods in Engineering*, *37*, 2527–2549.

Simo, J. C., & Wong, K. K. (1991). Unconditionally stable algorithms for rigid body dynamics that exactly preserve energy and momentum. *International Journal for Numerical Methods in Engineering*, *31*, 19–52.

Simo, J. C., Lewis, D., & Marsden, J. E. (1991). Stability of relative equilibria. Part I: The reduced energy-momentum method. *Archive for Rational Mechanics and Analysis*, *115*, 15–59.

Simo, J. C., Rifai, M. S., & Fox, D. D. (1992a). On a stress resultant geometrically exact shell model. Part VI: Conserving algorithms for non-linear dynamics. *International Journal for Numerical Methods in Engineering*, *34*, 117–164.

Simo, J. C., Tarnow, N., & Wong, K. K. (1992b). Exact energy-momentum conserving algorithms and symplectic schemes for nonlinear dynamics. *Computer Methods in Applied Mechanics and Engineering*, *100*, 63–116.

Tarnow, N. (1993). Energy and Momentum Conserving Algorithms for Hamiltonian Systems in the Nonlinear Dynamics of Solids. Ph.D. Dissertation, Sudam report no. 93–4. Stanford University.

Truesdell, C., & Noll, W. (2004). *The non-linear field theories of mechanics* (3rd ed.). Springer (2004).

http://www.springer.com/978-3-319-31877-6

Structure-preserving Integrators in Nonlinear Structural Dynamics and Flexible Multibody Dynamics

Betsch, P. (Ed.)
2016, VII, 291 p. 80 illus., 20 illus. in color., Hardcover
ISBN: 978-3-319-31877-6